arXiv:1511.00934v1 [astro-ph.SR] 3 Nov 2015

DETAILED ABUNDANCES OF STARS WITH SMALL PLANETS DISCOVERED BY *KEPLER* I: The First Sample*

Simon C. Schuler[1,11], Zachary A. Vaz[1], Orlando J. Katime Santrich[2], Katia Cunha[2,3], Verne V. Smith[2,4], Jeremy R. King[5], Johanna K. Teske[6,7], Luan Ghezzi[8], Steve B. Howell[9,11], AND Howard Isaacson[10]

ABSTRACT

We present newly derived stellar parameters and the detailed abundances of 19 elements of seven stars with small planets discovered by NASA's *Kepler* Mission. Each star save one has at least one planet with a radius $\leq 1.6\ R_{\oplus}$, suggesting a primarily rocky composition. The stellar parameters and abundances are derived from high signal-to-noise ratio, high-resolution echelle spectroscopy

*Some of the data presented herein were obtained at the W.M. Keck Observatory, which is operated as a scientific partnership among the California Institute of Technology, the University of California and the National Aeronautics and Space Administration. The Observatory was made possible by the generous financial support of the W.M. Keck Foundation.

[1]University of Tampa, Tampa, FL, 33606 USA; sschuler@ut.edu, zachary.vaz@spartans.ut.edu

[2]Observatório Nacional, Rio de Janeiro, RJ, Brazil; osantrich@on.br, kcunha@noao.edu, vsmith@noao.edu

[3]Steward Observatory, University of Arizona, Tucson, AZ 85721 USA

[4]National Optical Astronomy Observatory, Tucson, AZ, 85719 USA

[5]Department of Physics and Astronomy, Clemson University, Clemson, SC 29634 USA; jking2@clemson.edu

[6]Department of Terrestrial Magnetism, Carnegie Institution of Washington, Washington, DC 20015 USA; jteske@carnegiescience.edu

[7]Carnegie Origins Fellow, joint appointment between Carnegie DTM/OCIW

[8]Harvard-Smithsonian Center for Astrophysics, Cambridge, MA 02138 USA; lghezzi@cfa.harvard.edu

[9]NASA Ames Research Center, Moffett Field, CA 94035 USA; steve.b.howell@nasa.gov

[10]Department of Astronomy, University of California, Berkeley, CA 94720 USA; hisaacson@berkeley.edu

[11]Visiting Astronomer, Kitt Peak National Observatory, National Optical Astronomy Observatory, which is operated by the Association of Universities for Research in Astronomy (AURA) under cooperative agreement with the National Science Foundation.

obtained with the 10-m Keck I telescope and HIRES spectrometer using standard spectroscopic techniques. The metallicities of the seven stars range from -0.32 dex to +0.13 dex, with an average metallicity that is subsolar, supporting previous suggestions that, unlike Jupiter-type giant planets, small planets do not form preferentially around metal-rich stars. The abundances of elements other than iron are in line with a population of Galactic disk stars, and despite our modest sample size, we find hints that the compositions of stars with small planets are similar to stars without known planets and with Neptune-size planets, but not to those of stars with giant planets. This suggests that the formation of small planets does not require exceptional host-star compositions and that small planets may be ubiquitous in the Galaxy. We compare our derived abundances (which have typical uncertainties of $\lesssim 0.04$ dex) to the condensation temperature of the elements; a correlation between the two has been suggested as a possible signature of rocky planet formation. None of the stars demonstrate the putative rocky planet signature, despite at least three of the stars having rocky planets estimated to contain enough refractory material to produce the signature, if real. More detailed abundance analyses of stars known to host small planets are needed to verify our results and place ever more stringent constraints on planet formation models.

Subject headings: planetary systems – planets and satellites:formation – stars:abundances – stars:atmospheres – stars:individual(Kepler-20, Kepler-21, Kepler-22, Kepler-37, Kepler-68, Kepler-100, Kepler-130)

1. INTRODUCTION

One of the greatest surprises to emerge from the growing list of known exoplanets is the incredible diversity in both the planets themselves and in the architectures of the planetary systems. Discovered planets range in size from the sub-mercury Kepler-37b (Barclay et al. 2013) to objects that straddle the boundary between planets and brown dwarfs, e.g. XO-3b (Johns-Krull et al. 2008), with a radius nearly twice that of Jupiter and a mass approaching the deuterium-burning limit of 13 $M_{\rm J}$. Hundreds of stars with single planets having semi-major axes ranging from less than one hundredth of an AU (Kepler-78b, Sanchis-Ojeda et al. 2013) to more than 100 AU (Fomalhaut b, Kalas et al. 2008) are known, but most systems have two or more planets. While none of the systems discovered to date can truly be called Solar-System analogs, the seven-planet system Kepler-90 (Cabrera et al. 2014; Lissauer et al. 2014) comes closest, with its small planets on orbits interior to its larger, Jupiter-type giant

planets. The most incredible systems of all may be those with circumbinary planets, in which the planets orbit both stars of a binary system (e.g., Kepler-16, Doyle et al. 2011).

Significant research efforts have been focused on characterizing the discovered planetary systems with the goal of determining planet properties, constraining planet formation models, and providing input for asteroseismic analyses, among others. A critical component of these efforts has been the derivation of the stellar parameters, metallicities, and abundances of numerous elements of the host stars. It is now well established that Jupiter-type giant planets form more readily in metal-rich environments, the so-called *planet-metallicity* correlation (e.g., Santos et al. 2001; Fischer & Valenti 2005; Ghezzi et al. 2010a), with a typical offset of ~ 0.15 dex in the metallicities found for stars with giant planets and stars without known giant planets. It is now also becoming more well established that stars with small planets do not follow this planet-metallicity correlation and that indeed Neptune-size and smaller planets form at a range of metallicities (Udry et al. 2006; Sousa et al. 2008; Ghezzi et al. 2010a; Buchhave et al. 2012; Everett et al. 2013). The penultimate of these works, Buchhave et al. (2012), uses the automated spectral fitting routine Stellar Parameter Classification (SPC) to determine the stellar parameters (e.g., $T_{\rm eff}$, $\log g$, [m/H][12]) for 152 stars harboring 226 planet candidates (175 of which have radii less than that of Neptune) discovered by NASA's *Kepler* Mission. Two main conclusions are reached by the authors. One, planets with radii less than four Earth radii form around stars with a wide range of metallicities, ranging from -0.6 dex to +0.5 dex. Two, the average metallicity of stars having planets with radii less than four Earth radii is near solar (-0.01 ± 0.02 dex), which is significantly lower than that of stars with giant planets. Moreover, Buchhave & Latham (2015) recently find that stars that host small planets ($R < 1.7R_{\oplus}$) have the same average metallicity (-0.02 ± 0.02 dex) as stars without detected transiting planets. Wang & Fischer (2015), though, have suggested the planet-metallicity correlation is universal and does apply to small planets, although at a lower significance than larger Jupiter-type giant planets.

Buchhave et al. (2014) find that, based on a homogeneous analysis of more than 400 stars hosting 600 planets discovered by *Kepler*, planets may be categorized into three distinct populations defined by the metallicities of the host stars. The authors suggest that small, rocky planets ($R < 1.7R_{\oplus}$) are found around stars with an average metallicity of [m/H] $= -0.02 \pm 0.02$, the slightly larger gas dwarf planets ($1.7R_{\oplus} < R < 3.9R_{\oplus}$) around stars with an average metallicity of [m/H] $= +0.05 \pm 0.01$, and the gas giant planets ($R > 3.9R_{\oplus}$) around stars with an average metallicity of [m/H] $= +0.18 \pm 0.02$. Their main conclusion is

[12]SPC gives the metallicity ([m/H]) in terms of the average abundance of all elements other than H and He, as opposed to the metallicity ([Fe/H]) based on the Fe content of the star, as is more common. Following Torres et al. (2012), we assume the two are equivalent throughout the paper.

that host star metallicity, and thus by proxy the protoplanetary disk metallicity, is a primary determinant of the final masses and compositions of small planets. In contrast, Schlaufman (2015) argues that there is no evidence for such discrete planet formation regimes, citing possible shortcomings in the Buchhave et al. (2014) analysis, and that it is more likely that a continuum of planet sizes from 1 $R_\oplus$ to 4 $R_\oplus$ form independent of host star metallicity. Therefore, Schlaufman's main conclusion is that host star and protoplanetary disk metallicity is unlikely to have a primary influence on the final masses and compositions of small planets.

Potentially more interesting is what the abundances of individual elements can inform us about the formation of planets, as recently demonstrated by Santos et al. (2015) who has shown that host star abundances can be used to constrain the compositions of orbiting rocky planets. For instance, the abundance of Li has been found to be depleted in stars hosting giant planets (e.g. Israelian et al. 2009; Delgado Mena et al. 2014), although there is some disagreement on whether the depleted abundances are due to planet formation or not (e.g. Ghezzi et al. 2010b; Ramírez et al. 2012). Adibekyan et al. (2012a) find that the abundances of α-elements are enhanced in metal-poor stars with rocky planets, suggesting that small planet formation is more efficient in environments enhanced with metals other than Fe. It also has been suggested that the formation of small, rocky planets may leave a chemical imprint in their host stars. Meléndez et al. (2009) reported that the refractory elements, those elements with condensation temperatures ($T_{\rm c}$) greater than 900 K, are depleted in the solar photosphere compared to nearby solar twins and analogs, and that the depletions are a function of $T_{\rm c}$, i.e., elements with higher $T_{\rm c}$ are increasingly more depleted. The authors suggest that the "missing" refractory elements are contained in the four rocky planets of our Solar System. Ramírez et al. (2009) were the first to look for this rocky planet signature in stars other than the Sun by deriving detailed abundances of 64 solar twins and analogs, and measuring the slope of a linear least-square fit to the refractory abundances as a function of $T_{\rm c}$. They found that $\simeq 15\%$ of the stars with [Fe/H] ≤ 0.1 have slopes that are consistent with depleted refractory elements.

Numerous studies have since investigated the putative rocky planet signature by analyzing additional solar twins and analogs with and without known planets, stars with known Jupiter-type giant, Neptune-type, and super-Earth planets, and late F-type dwarf stars. In general, most studies find stars with slopes indicative of depleted refractories and stars with slopes that are not, but there are substantive differences in the interpretations of the observed slopes. Ramírez et al. (2010); Meléndez et al. (2012), and Ramírez et al. (2014, 2015) argue that refractory depletions that they observe are in fact due to rocky planet formation. González Hernández et al. (2010, 2013) find no evidence that [x/Fe]-$T_{\rm c}$ trends are related to the presence of rocky planets. Önehag et al. (2011) find an abundance pattern similar to that of the Sun in a solar twin in the M67 open cluster and suggest the depleted

refractories in both stars may be due to radiative dust cleansing by nearby luminous stars during their formation; a follow-up study of additional M67 stars reaches the same conclusion (Önehag et al. 2014). Schuler et al. (2011) show that Galactic chemical evolution may be responsible for the depleted refractories they find in a sample of stars with Jupiter-type giant planets. Adibekyan et al. (2014) conclude that the age and Galactic birthplace of a star determine its chemical composition and suggest that planet formation does not deplete refractory elements from host stars. Maldonado et al. (2015) studied the abundances of stars with and without circumstellar debris discs and found no differences in the compositions of the two; furthermore, they find that stars with debris discs and low-mass planets have compositions similar to stars with no detected planets. Finally, Nissen (2015) derived detailed abundances for a sample of solar twins and concludes that the interpretation of [x/Fe]-$T_{\rm c}$ trends is complicated because of the convoluted effects of planet formation or dust-gas segregation, stellar age, and Galactic chemical evolution. Gaidos (2015) has also recently argued that dust-gas segregation is a plausible explanation for the [x/Fe]-$T_{\rm c}$ trends.

As the discord among these various studies demonstrates, it is yet unclear if [x/Fe]-$T_{\rm c}$ trends are indicative of rocky planet formation. However, it is important to emphasize that aside from the fine analysis of the Sun by Meléndez et al. (2009), none of the studies discussed above have included stars with known Earth-like rocky planets. We have undertaken a concerted effort to address this issue by targeting stars with known rocky planets discovered by *Kepler*. Here, as a first step, we present the results of a detailed abundance analysis of seven *Kepler* stars, six of which have at least one planet with a radius less than or approximately equal to 1.6 $R_{\oplus}$, and thus their detailed abundances presented here are important contributions to the ongoing efforts to characterize small planet host stars. We compare the abundances of each star to a general population of Galactic disk stars in order to place them into a larger context. We also analyze the refractory element abundances as a function of $T_{\rm c}$ to test the hypothesis that rocky planet formation leaves an observable signature in the composition of the host stars.

2. OBSERVATIONS AND DATA REDUCTIONS

We have analyzed high-resolution, high-signal-to-noise (S/N) ratio spectra of seven stars, each of which has at least one confirmed small planet discovered by *Kepler*. The stars are:

Kepler-20: a G8 V[13] dwarf with an age of $8.8^{+4.7}_{-2.7}$ Gyr and host of five known planets (Gautier et al. 2012; Fressin et al. 2012). Kepler-20e and Kepler-20f have radii of $0.868^{+0.074}_{-0.096}$ $R_{\oplus}$ and $1.03^{+0.10}_{-0.13}$ $R_{\oplus}$, respectively, and thus are considered Earth-size planets. Kepler-20b has a radius of $1.91^{+0.12}_{-0.21}$ $R_{\oplus}$ and is classified as a super-Earth. The remaining two plan-

ets, Kepler-20c and Kepler-20d, have been labeled as sub-Neptunes ($R_{\rm Neptune} = 3.88\ R_\oplus$) with radii of $3.07^{+0.20}_{-0.31}\ R_\oplus$ and $2.75^{+0.17}_{-0.30}\ R_\oplus$, respectively. Only the masses of Kepler-20b ($M_{\rm b} = 8.7^{+2.1}_{-2.2}\ M_\oplus$) and Kepler-20c ($M_{\rm c} = 16.1^{+3.3}_{-3.7}\ M_\oplus$) have been determined definitively (Gautier et al. 2012).

Kepler-21: a F6 IV[13] subgiant with an age of 2.84 ± 0.34 Gyr and host of one known planet (Howell et al. 2012). Kepler-21b has a radius of $1.64 \pm 0.04\ R_\oplus$ and is classified as a super-Earth. A definitive mass has yet to be determined for this planet.

Kepler-22: a G5 V[14] dwarf without a well-determined age and host to one known planet (Borucki et al. 2012). Kepler-22b has a radius of $2.38 \pm 0.13\ R_\oplus$ and is classified as a sub-Neptune. A definitive mass has yet to be determined for this planet.

Kepler-37: a main-sequence (MS) dwarf of undetermined spectral type with an age of 5.66 Gyr (Marcy et al. 2014b, no uncertainty provided) and host to three known planets (Barclay et al. 2013). Kepler-37b is a sub-Mercury-size planet with a radius of $0.303^{+0.053}_{-0.073}\ R_\oplus$. Kepler-37c is a Earth-size planet with a radius of $0.742^{+0.065}_{-0.083}\ R_\oplus$, and Kepler-37d is a super-Earth with a radius of $1.99^{+0.11}_{-0.14}\ R_\oplus$. Definitive masses have yet to be determined, but Marcy et al. (2014b) estimate masses of $M_{\rm b} = 2.78 \pm 3.7\ M_\oplus$, $M_{\rm c} = 3.35 \pm 4.0\ M_\oplus$, and $M_{\rm d} = 1.87 \pm 9.08\ M_\oplus$ for the three planets using a posterior distribution based on a Markov-Chain-Monte-Carlo routine.

Kepler-68: a MS dwarf of undetermined spectral type with an age of 6.3 ± 1.7 Gyr and host to three known planets (Gilliland et al. 2013). The two inner planets, Kepler-68b and Kepler-68c, are a sub-Neptune with a radius of $2.31^{+0.06}_{-0.09}\ R_\oplus$ and a Earth-size planet with a radius of $0.953^{+0.037}_{-0.042}\ R_\oplus$, respectively. Follow-up RV measurements of Kepler-68 revealed a third, Jupiter-type giant planet, Kepler-68d, orbiting beyond the two inner planets. The initial RV measurements yielded a mass of $M_{\rm b} = 8.3^{+2.2}_{-2.4}\ M_\oplus$ for Kepler-68b and a minimum mass of $M \sin i = 0.947 \pm 0.035\ M_J$ for Kepler-68d (Gilliland et al. 2013). Analysis of additional RV data refined these values to $M_{\rm b} = 5.97 \pm 1.7\ M_\oplus$ and $M \sin i = 0.84 \pm 0.006\ M_J$, respectively (Marcy et al. 2014b). A definitive mass has yet to be determined for Kepler-68c.

Kepler-100: a MS dwarf of undetermined spectral type with an age of 6.5 Gyr and host to three known planets (Marcy et al. 2014b). Kepler-100b and Kepler-100d have radii of $1.32 \pm 0.04\ R_\oplus$ and $1.61 \pm 0.05\ R_\oplus$, respectively, and thus are classified as super-Earths. Kepler-100c, a sub-Neptune, has a radius of $2.20 \pm 0.05\ R_\oplus$. Definitive masses have yet to be determined, but Marcy et al. (2014b) estimate masses of $M_{\rm b} = 7.34 \pm 3.2\ M_\oplus$ and

[13]http://simbad.u-strasbg.fr/simbad/sim-fid

[14]http://exoplanetarchive.ipac.caltech.edu/

$M_c = 0.85 \pm 4.0\ M_\oplus$ for Kepler-100b and Kepler-100c, respectively.

Kepler-130: a MS dwarf of undetermined spectral type without a well-determined age and host to three known planets (Rowe et al. 2014). Kepler-130b is an Earth-size planet with a radius of $1.02 \pm 0.04\ R_\oplus$, and Kepler-130d is a super-Earth with a radius of $1.64 \pm 0.16\ R_\oplus$. Kepler-130c is classified as a sub-Neptune with a radius of $2.81 \pm 0.09\ R_\oplus$. Definitive masses have yet to be determined for these planets.

The spectra of these stars were obtained as part of the *Kepler* Follow-up Observing Program (KFOP), an effort orchestrated by *Kepler* science team members to confirm planetary candidates discovered by *Kepler* and to characterize the planetary systems and their host stars. The 10-m Keck I telescope and High Resolution Echelle Spectrometer (HIRES; Vogt et al. 1994) are being utilized for precise RV measurements of high-priority KOIs in order to confirm bona fide planets and to place constraints on their masses. Precise RVs of the host stars are made possible by the insertion of an iodine cell into the spectrometer's light path, superimposing the iodine spectrum on the stellar spectrum and providing a stable spectral reference against which subtle shifts in the stellar spectrum can be measured. The iodine reference spectrum is dense with absorption lines from approximately 5000 – 6300 Å (Marcy & Butler 1992) and makes the stellar spectrum unusable in this region for abundance analysis. Instead, we use the template spectra– spectra of the target stars taken with the same instrumental setup but without the iodine cell– for our abundance analysis. Moreover, only stars with spectra having S/N ratios per pixel greater than 150 were considered for study. The instrumental setup, observational procedure, and data reduction used for the KFOP targets are the same as those used by the California Planet Search survey (Marcy et al. 2008). The KFOP spectra are characterized by a spectral resolution of $R = \lambda/\Delta\lambda = 50,000$ and span 3650 – 7950 Å with incomplete coverage in the reddest orders.

Additional observations of Kepler-21 were made independently with Keck/HIRES and the 4-m Mayall telescope and echelle spectrograph at Kitt Peak National Observatory (KPNO) in UT 2011. The Keck/HIRES observations were made with a different instrumental setup than those of the KFOP. The setup included a cross-disperser angle of 0.102, an echelle angle of 0.000, the C1 decker, and a projected slit width of 0.86". This setup provided a nominal resolution of $R = 50,000$ and a wavelength coverage from 3750 to 8170 Å that is incomplete in the reddest orders. These Keck/HIRES spectra were reduced with the MAKEE[15] data reduction package, which was developed specifically for HIRES data. MAKEE is an automated pipeline that carries out the typical reduction procedures, including bias correction, flat fielding, order extraction, and wavelength calibration.

[15]http://spider.ipac.caltech.edu/staff/tab/makee/index.html

The KPNO spectrum was obtained during engineering time with the 4-m Mayall telescope. The echelle spectrograph was setup with the $58.5\,\mathrm{g\,mm^{-1}}$ echelle grating and $226 - 1\,\mathrm{g\,mm^{-1}}$ cross disperser, resulting in a wavelength coverage of 5270 – 8060 Å with incomplete spectral coverage in the reddest orders. A projected slit width of 1" produced a spectral resolution of $R \sim 42,000$. The T2KA ccd detector with 2048×2048 pixels was used. Standard routines within the IRAF[16] image processing software were used for the data reductions, which included bias removal, scattered light subtraction, flat fielding, order extraction, and wavelength calibration. Details of all observations, including the S/N ratios of the spectra, are given in the Observing Log (Table 1). Sample spectra are shown in Figure 1.

3. ABUNDANCE ANALYSIS & RESULTS

Our abundance analysis follows that described in Schuler et al. (2011) and includes the derivation of stellar parameters ($T_{\rm eff}$, $\log g$, and microturbulent velocity [ξ]) for each star in addition to the abundances of up to 19 elements via an LTE, curve-of-growth analysis. The abundances have been derived by means of equivalent width (EW) measurements of spectral absorption lines and by the spectral synthesis fitting technique, depending on the line considered. The lines analyzed are drawn from the line list described in Schuler et al. (2011). The one-dimensional spectrum analysis package SPECTRE (Fitzpatrick & Sneden 1987) was used to measure EWs, primarily utilizing Gaussian profiles; for strong lines (EW $\gtrsim$ 90 mÅ) with broad wings near the continuum, Voigt profiles were used for the fits. The 2014 version of the LTE spectral analysis software package MOOG (Sneden 1973) was used to derive the abundances from the measured EWs and the synthetic fits to the data using model atmospheres interpolated from the extensive grids of Kurucz ATLAS9[17] models with convective overshoot. Final abundances are reported relative to solar abundances that have been derived in the exact same manner as those for the *Kepler* stars using solar spectra obtained with the same instrumental configurations on the Keck and KPNO 4-m telescopes, and adopting the solar parameters $T_{\rm eff}$= 5777 K, $\log g = 4.44$, and $\xi = 1.38$ km s^{-1}. The one exception is the relative abundances for Kepler-21 derived from the Keck (non-KFOP) spectrum. No solar spectrum was obtained during the observing run, so abundances derived from the KFOP solar spectrum have been used instead.

[16]IRAF is distributed by the National Optical Astronomy Observatory, which is operated by the Association of Universities for Research in Astronomy, Inc., under cooperative agreement with the National Science Foundation.

[17]See http://kurucz/harvard.edu/grids.html

3.1. Stellar Parameters

Stellar parameters for each star have been derived directly from the spectra using excitation and ionization balance of Fe I and Fe II. Initial parameters for each star were taken from the planet validation papers as listed in the Introduction. The parameters were then altered until no correlation existed between the derived [Fe I/H] and lower excitation potential (χ) and [Fe I/H] and reduced EW [log(EW/λ)] for each Fe I line measured, and until the [Fe/H] abundances derived from Fe I and Fe II lines were equal to within two significant digits. Deriving stellar parameters in this way results in unique solutions only if there is no ab initio correlation between χ and EW of the measured Fe I lines. Such correlations did exist for the initial Fe I line lists for Kepler-20, Kepler-22, and Kepler-37, but the correlations were eliminated by removing two, four, and seven Fe I lines from their respective line lists. Uncertainties in $T_{\rm eff}$ and ξ are the differences in the adopted parameters and those that result in 1σ correlations in the [Fe/H] versus χ and reduced EW relations, respectively. The derived surface gravities are sensitive to the Fe abundance derived from both Fe I and Fe II lines, with a greater sensitivity to the latter, and thus the uncertainty in $\log g$ is dependent on the uncertainty in the Fe abundances, as more fully described in Bubar & King (2010).

The derived stellar parameters, Fe abundances, and their uncertainties are given in Table 2. Parameters and Fe abundances have been derived for Kepler-21 from each of the three spectra– KFOP, Keck (non-KFOP), and KPNO– obtained for this star. The results from the three different spectra are indistinguishable within the combined uncertainties, with those from the KFOP and Keck observations in particularly good agreement: $\Delta T_{\rm eff} = -52$ K, $\Delta \log g = -0.09$, and Δ[Fe/H] $= -0.02$. This is reassuring given the spectra were taken with the same telescope and spectrograph. The $\log g$ derived from the KPNO spectroscopy deviates from the KFOP and Keck values by 0.28 and 0.19 dex, respectively. While the differences are approaching statistical significance, they are readily understood given the significantly lower S/N of the KPNO spectrum compared to the Keck and KFOP spectra, as well as the small number of Fe II lines, and thus higher uncertainty in the mean [Fe II/H] abundance, measurable in the KPNO spectrum. The adopted stellar parameters and Fe abundances for Kepler-21 are those derived from the Keck (non-KFOP) spectrum and have been used in the derivation of the other elements. All additional references to the parameters of Kepler-21 will refer to these adopted values.

3.2. Abundances

The abundances of individual elements that require special attention are described in the subsections that follow. The stellar and solar EW measurements and the respective

absolute abundance for each line of all elements analyzed are given in the Appendix. The final adopted abundances, given relative to the solar, and their uncertainties for each star are provided in Table 3.

3.2.1. Lithium

Li abundances have been derived from the λ6707 Li resonance feature using spectral synthesis. The adopted line list is that from King et al. (1997) updated as described in Schaeuble & King (2012). The synthetic spectra were smoothed using Gaussian profiles with full widths at half maximum (FWHM) determined from weak, unblended absorption lines in the same spectral order as the Li feature. Sample spectra and fits of the λ6707 Li region are given in Figure 2.

3.2.2. Carbon and Oxygen

Abundances of the light elements C and O have been derived from a combination of atomic and molecular lines. For C, we make use of five high-excitation C I lines and two C_2 features. Formation of high-excitation C I lines is susceptible to non-LTE effects, but abundances derived from the lines measured here have been shown to be largely free of deviations from the LTE approximation for solar-type stars (Asplund et al. 2005; Takeda & Honda 2005). The two C_2 features (λ5086 and λ5136) are blends of multiple components of the C_2 Swan system; spectral synthesis was used to derive C abundances from these features. The final adopted C abundance for each star is the mean of the relative abundances derived from the C I and C_2 lines, except for Kepler-21, for which only C I lines were measurable, and for Kepler-37, for which the mean abundance derived from the C I lines is 0.16 dex higher than that derived from the C_2 lines. Abundances derived from high-excitation lines, in particular the λ7775 high-excitation O I triplet ($\chi = 9.15$ eV) and λ6053 S I line ($\chi = 7.87$ eV), using one-dimensional LTE analyses have been shown to increase dramatically with decreasing $T_{\rm eff}$ in stars with $T_{\rm eff} \lesssim 5400$ K, contrary to canonical NLTE predictions (Schuler et al. 2004, 2006; Ramírez et al. 2013; Teske et al. 2013). Similar increases in Fe abundances derived from Fe II lines relative to Fe I lines are seen in the same temperature regime (Schuler et al. 2003; Yong et al. 2004; Schuler et al. 2010). Taken together, the overabundances derived from high-excitation and singly ionized lines in the spectra of cool stars suggest that the electron populations of these energy states are not accurately modeled by our standard LTE analysis. We suspect that the difference in C I ($\chi = 7.68, 8.65$ eV) and C_2 abundances of Kepler-37, with $T_{\rm eff} = 5406$ K, is due to the overpopulation of the high-excitation C I states

and thus adopt the C_2 based abundances for this star. The C abundances of all the stars are given in Table 4.

The abundances of O have been derived from the λ6300 forbidden [O I] line and the λ7775 high-excitation O I triplet. The λ6300 line is blended with two isotopic components of a Ni I transition at 6300.34 Å for which account must be taken when deriving O abundances from this feature. We use the blends driver within the MOOG software package for this purpose. The necessary input for the abundance derivation includes the EW of the λ6300 feature, atomic parameters (χ and $\log gf$) for both the O and Ni transitions, and a Ni abundance. The atomic parameters for the [O I] line are taken from the fine analysis of Allende Prieto et al. (2001); those for the Ni blend are from the laboratory analysis of Johansson et al. (2003). The adopted Ni abundances are those derived here and given below. Unlike the λ6300 forbidden [O I] line which has been shown to be well described by LTE (e.g., Takeda 2003), formation of the high-excitation O I triplet is sensitive to NLTE effects (e.g., Kiselman 1991). NLTE corrections for the O I triplet based abundances have been estimated using the analytical formula provided by (Takeda 2003). We also tested the NLTE corrections of Fabbian et al. (2009), which cover a smaller parameter space compared to Takeda et al. The corrections are found to be similar for stars falling within the parameter space of both studies.

The derived O abundances are provided in Table 5, where it can be seen that the [O I] and the NLTE-corrected O I triplet abundances are in good agreement for Kepler-20 and Kepler-21. Because we consider the [O I]-based abundances to be more reliable, they are adopted as the final O abundances for these two stars. The [O I] line was not measurable in the Kepler-22, Kepler-68, Kepler-100, and Kepler-130 spectra, so the NLTE-corrected triplet-based abundances are adopted for these stars. We note, however, that the NTLE corrections for Kepler-22 and Kepler-68 are expected to be of the same order as for the Sun (Takeda 2003), so the LTE and NLTE abundances should not differ significantly. This is indeed observed, as the LTE and NLTE-based abundances differ by only a few dex in each case (Table 5). Both the [O I] and O I triplet features were measurable for Kepler-37, but as described above, the triplet based abundance is likely unreliable due to the overpopulation of high-excitation states in this cool star. We therefore adopt the [O I] based abundance as the final O abundance for Kepler-37.

3.2.3. Odd-Z Elements: Sc, V, Mn, and Co

The line profiles of the odd-Z elements Sc, V, Mn, and Co can be affected by hyperfine structure (hfs) in some of the electron transitions of these atoms, resulting in enhanced

abundances of these elements if not modeled properly. However, hfs is expected to be significant only in transitions that result in large EWs ($\gtrsim$ 50 mÅ; Prochaska & McWilliam 2000). We inspected the EW and relative abundance of each line of these elements for all the stars in our sample, and the abundances of Sc, V, and Co show no indication of being affected by hfs. The Mn abundances of Kepler-20 and Kepler-37, on the other hand, are indicative of hfs effects. For Kepler-20, the EWs of the two measured Mn lines are 55.8 mÅ (λ5400) and 83.5 mÅ (λ5433), and the resulting relative abundances are 0.10 dex and 0.29 dex higher, respectively, than the star's mean metallicity. For Kepler-37, the λ5433 line, with an EW of 61.6 mÅ, shows a slight abundance enhancement of 0.13 dex compared to the λ5400 line, which has an EW of only 28.0 mÅ and a relative abundance in agreement with the star's mean metallicity.

Corrected Mn abundances of Kepler-20 and Kepler-37 were determined by using spectral synthesis and the hfs components of the λ5433 line compiled by Johnson et al. (2006) combined with a line list of surrounding features from the Vienna Atomic Line Database (VALD, Kupka et al. 1999, 2000; Ryabchikova et al. 1997; Piskunov et al. 1995). To achieve consistent relative abundances, the λ5433 line was also synthesized for the Sun. The hfs-corrected abundance for Kepler-20, [Mn/H] = +0.04, is 0.31 dex lower than the non-corrected value and 0.12 dex lower than the abundance derived from the λ5400 line. The hfs-corrected abundance only is adopted for Kepler-20. For Kepler-37, the hfs-corrected abundance, [Mn/H] = −0.35, is only 0.05 dex lower than the non-corrected abundance, signifying that it is only slightly affected by hfs. Nonetheless, we adopt this hfs-corrected value and combine it with that of the λ5400 line, which is not expected to be affected by hfs, to obtain the adopted Mn abundance ([Mn/H] = −0.39) for Kepler-37.

3.2.4. Abundance Uncertainties

Uncertainties in the derived stellar parameters ($T_{\rm eff}$, $\log g$, and ξ) and the uncertainty in the mean abundance (σ_μ) of a given element contribute to the total internal uncertainty in the derived abundance of that element. For elements whose abundances are based on two or less lines, the total uncertainty is based on the parameter uncertainties alone. Abundance sensitivities to the stellar parameters were determined for each star by calculating changes in the final abundances due to parameter changes of ±150 K in $T_{\rm eff}$, ±0.25 dex in $\log g$, and ±0.30 km s^{-1} in ξ; representative sensitivities are given in Table 6. Abundance uncertainties to each parameter are then calculated by scaling the abundance sensitivities by the uncertainty in the respective stellar parameter. The final total internal uncertainty is the quadratic sum of the individual uncertainties due to the stellar parameters and σ_μ, for those

elements with abundances derived from more than two lines.

4. DISCUSSION

4.1. Comparison to Previous Results

Accurately derived stellar parameters are essential for the characterization of exoplanets and as asteroseismic inputs. *Kepler*'s incredible success at finding planetary candidates during its primary mission has dramatically increased the number of stars for which effective temperatures, surface gravities, and metallicities are needed in short order, so the size and equilibrium temperature of the planet(s) can be accurately determined. Automated (spectrum fitting) and semi-automated (spectral line synthesis) routines, such as Spectroscopy Made Easy (SME; Valenti & Piskunov 1996), SPC (Buchhave et al. 2012), Automatic Routine for line Equivalent widths in stellar Spectra (ARES; Sousa et al. 2007), and Versatile Wavelength Analysis (VWA; Bruntt et al. 2002) to name a few, are generally used to meet this demand. In Table 7 we compare results in the existing literature to ours derived by "by hand" to provide a check of those determined using automated or semi-automated routines, and to ensure that the most accurate stellar parameters are being used in planetary characterization and asteroseismic studies. Here we discuss the comparisons for each star.

Kepler-20: Stellar parameters and metallicities have been derived for Kepler-20 by Gautier et al. (2012) and Fressin et al. (2012), both of which employed SME using the same Keck/HIRES spectrum obtained as part of the KFOP. The two studies find nearly identical parameters and metallicity for this star. The $T_{\rm eff}$ and [Fe/H] of both studies are in agreement with ours within uncertainties, and the surface gravity values are the same at $\log g = 4.44$.

Kepler-21: Numerous spectroscopic and asteroseismic studies have determined the stellar parameters and metallicity of Kepler-21. Howell et al. (2012) carried out an extensive spectroscopic study of the star, analyzing three separate spectra obtained with three different telescopes. Stellar parameters and metallicities were determined from each spectrum using automated spectrum-fitting routines and compared to existing literature values. The final adopted parameters and metallicity were chosen from the accumulated data set. Molenda-Żakowicz et al. (2013) derived two sets of parameters and metallicities using two different routines: the spectrum fitting package ROTFIT (Frasca et al. 2003) and the semi-automated routine ARES along with MOOG. The two sets of results, with the exception of the metallicities, differ at greater than the 1σ level, with the ARES/MOOG results being particularly disparate; it is the only analysis suggesting that Kepler-21 has the surface gravity of a MS dwarf rather than a subgiant. Everett et al. (2013) developed a spectrum-fitting

routine to analyze low-resolution ($R \sim 3000$) spectra obtained with the KPNO 4-m Mayall telescope and RCSpec long-slit spectrograph. Bruntt et al. (2012) used the semi-automated routine VWA to derive $T_{\rm eff}$, metallicity, and the abundances of 11 other elements, all of which are included in our analysis. The stellar parameters and metallicities of Howell et al. (2012), Bruntt et al. (2012), and the ROTFIT analysis of Molenda-Żakowicz et al. (2013) are in agreement with ours within uncertainties, while the stellar parameters of Everett et al. (2013), based on low-resolution spectroscopy, are lower by more than the combined uncertainties. Also, the abundances of the eleven additional elements derived by Bruntt et al. (2012) are in good agreement with our results, with all of them agreeing within uncertainties except for the abundance of carbon, our abundance (-0.02 ± 0.05) for which is +0.18 dex higher than theirs (-0.20 ± -0.07).

Asteroseismic analyses generally require $T_{\rm eff}$ and [Fe/H] as input, and they determine the fundamental stellar properties of mass, radius, and density. With the mass and radius, the surface gravity of a star can be accurately determined (e.g., Chaplin & Miglio 2013). No less than five different papers report fundamental properties of Kepler-21 based on asteroseismology, and three of the analyses include deriving the input $T_{\rm eff}$ and [Fe/H] parameters themselves, either from high-resolution spectroscopy or photometry (Howell et al. 2012; Silva Aguirre et al. 2012, 2015), one adopts the parameters from the literature (Mathur et al. 2012), and one does both (Chaplin et al. 2014). The derived $T_{\rm eff}$ values from these studies range from 5838 K to 6305 K, and the [Fe/H] values from -0.20 to -0.01. Our adopted $T_{\rm eff}$ (6177 ± 42 K) and [Fe/H] (-0.08 ± 0.07) fall nicely in the middle of these ranges. More impressive is the tight agreement in the asteroseismically derived surface gravities, which range from 4.0 dex to 4.03 dex, despite the large ranges in $T_{\rm eff}$ and [Fe/H]. Our adopted surface gravity, $\log g = 3.99 \pm 0.15$, is in near-perfect agreement with these values.

Kepler-22: Two sets of stellar parameters and metallicities have been derived for Kepler-22 by Borucki et al. (2012). One analysis utilized SME and a Keck/HIRES KFOP spectrum, and the other combined the results of spectrum-fitting analyses of five separate spectra obtained with four different telescopes. Borucki et al. (2012) also carried out an asteroseismic analysis, and Huber et al. (2014) calculate a surface gravity based on former's derived mass and radius. Both sets of spectroscopic results are in good agreement with ours, with only $T_{\rm eff}$ from the SME analysis deviating from our value by more than the combined uncertainties. Also, our derived surface gravity is 0.13 dex higher, just larger than the combined uncertainty, than the asteroseismically derived value.

Kepler-37: Stellar parameters and metallicity of Kepler-37 are reported in the Kepler-37b discovery paper, Barclay et al. (2013). They used SME and SPC to analyze two sets of spectra obtained from two different telescopes as part of the KFOP. After deriving initial

parameters and metallicity, asteroseismology was used to determine the star's surface gravity, among other things, and then the surface gravity was held fixed while $T_{\rm eff}$ and [Fe/H] were rederived. The final adopted values are the averages of those from the SME and SPC analyses. The Buchhave et al. (2012) values are in excellent agreement with those of Barclay et al., and both sets of results agree with our derived values within the uncertainties. Everett et al. (2013) also analyzed a low-resolution Mayall/RCSpec spectrum of this star. While their surface gravity agrees with ours within the uncertainties, their $T_{\rm eff}$ and [Fe/H] are lower than ours by more than the combined uncertainties. Finally, our surface gravity, as well as those of Barclay et al. (2013) and Buchhave et al. (2012), is in good agreement with the asteroseismic value of Silva Aguirre et al. (2015).

Kepler-68: Gilliland et al. (2013) determined the stellar parameters and metallicity of Kepler-68 using SME and a KFOP spectrum with the surface gravity constrained by an asteroseismic analysis, similar to the analysis of Barclay et al. (2013). These results are in good agreement with the Buchhave et al. (2012) values, all of which agree within the uncertainties. The surface gravities are also in agreement with the asteroseismic value determined by Silva Aguirre et al. (2015). While the results of Gilliland et al. (2013) agree with ours within the combined uncertainties, the stellar parameters of Buchhave et al. (2012) and the surface gravity of Silva Aguirre et al. (2015) differ from ours by slightly more than the combined uncertainties, with our values larger than those of these two studies. Despite these differences, the metallicities are in very good agreement.

Kepler-100: Initial stellar parameters without uncertainties for Kepler-100 are provided by Batalha et al. (2013) based on an SME analysis of a KFOP spectrum. Refined stellar parameters and a metallicity were derived by Marcy et al. (2014b) using SME and a KFOP spectrum with the surface gravity constrained by an asteroseismic analysis, similar to the analysis of Barclay et al. (2013). These updated results are in good agreement with those of Buchhave et al. (2012). The surface gravities also match well the asteroseismic value of Silva Aguirre et al. (2015). The results of the latter three studies are in agreement with ours within the combined uncertainties, but those of Batalha et al. (2013) differ by more than the uncertainties of our analysis.

Kepler-130: Stellar parameters and metallicity of Kepler-130 have been derived by Huber et al. (2013) using either SME or SPC and a KFOP spectrum (which routine and the source of the spectrum is not specified for individual stars) with the surface gravity constrained by an asteroseismic analysis, similar to the analysis of Barclay et al. (2013). These results are near perfect agreement with those of Buchhave et al. (2012), and both sets of results agree with ours within the combined uncertainties.

Overall, the statistical agreement between our derived stellar parameters and metallic-

ities of these *Kepler* host stars and those derived by numerous other groups using various automated and semi-auotmated routines with *high-resolution spectroscopy* is quite good. Only the ARES/MOOG stellar parameters of Kepler-21 (Molenda-Żakowicz et al. 2013), the SME $T_{\rm eff}$ of Kepler-22 (Borucki et al. 2012), the SPC stellar parameters of Kepler-68 (Buchhave et al. 2012), and the initial SME stellar parameters of Kepler-100 (Batalha et al. 2013) differ from our values by more than the combined uncertainties. In each case, the metallicity of each analysis agrees with ours. In contrast to the high-resolution spectroscopic analyses, the low-resolution spectroscopic analysis of Everett et al. (2013) produces more disparate results for the $T_{\rm eff}$ and $\log g$ of Kepler-21, and the $T_{\rm eff}$ and [Fe/H] of Kepler-37, all of which are underestimated at greater than the 2σ level. Nonetheless, the low-resolution spectroscopic results are considered to be an improvement over the photometrically derived stellar parameters and metallicities given in the *Kepler* Input Catalog (Brown et al. 2011).

It is also encouraging that our surface gravities statistically agree with the asteroseismic values for four of the six stars in our sample. For the two stars, Kepler-22 and Kepler-68, whose surface gravities are not in agreement, our values are larger at about the 1.7σ level in each case. It is generally accepted that asteroseismology provides the most accurate and precise surface gravities, because they are largely independent of the input stellar physics (Chaplin & Miglio 2013). It has been shown that, in general, $\log g$ determined spectroscopically by forcing ionization balance are larger than asteroseismically determined values, with the difference increasing with increasing $T_{\rm eff}$ (e.g., Mortier et al. 2014). While not all of the stars in our sample follow this general trend, it does agree with what we find for Kepler-22 and Kepler-68. The source of the discrepancy is not yet fully understood and merits further investigation. Nonetheless, our derived $T_{\rm eff}$ and [Fe/H] remain robust, because they do not correlate with changes in $\log g$ for standard curve-of-growth analyses (Torres et al. 2012; Mortier et al. 2014). Furthermore, based on the derived sensitivities (Table 6), the abundances of the other elements should also not be greatly affected by our slightly overestimated $\log g$ for Kepler-22 and Kepler-68.

4.2. The Abundances of Stars with Small Planets

An immediate conclusion that can be drawn from the abundances given in Table 3 is that small planets (in this case, $0.30\ R_\oplus \lesssim R \lesssim 3.00\ R_\oplus$) form in environments with a range of metallicities, from metal-poor ([Fe/H] ≈ -0.30) to metal-rich ([Fe/H] $\approx +0.15$). This is in concordance with previous suggestions based on stars with planets classified as sub-Neptunes (Udry et al. 2006; Sousa et al. 2008; Ghezzi et al. 2010a) and, in particular, small planet candidates discovered by *Kepler* (Buchhave et al. 2012; Everett et al. 2013;

Buchhave & Latham 2015). We point out that at the time of this writing that at least 145 of the 226 planet candidates in the Buchhave et al. (2012) sample, including those discussed herein, have since been confirmed as bona fide planets (according to *Kepler*'s Table of Confirmed Planets[18]), making more robust their conclusions that small planets form around stars with a wide range of metallicities and that the average metallicity of stars with small planets is approximately solar. Interestingly, the star with the highest metallicity, Kepler-68, is the one star in our sample with a known Jupiter-type giant planet.

Beyond the bulk metallicity of the host stars, the abundances of 15 of the remaining 18 other elements derived for each star show no deviations from general Galactic abundance distributions. In Figure 3 we compare the abundances of each element relative to Fe for the stars in our sample to those from studies that have analyzed a large number of stars with and without detected planets in the Galactic disk. Carbon and oxygen abundances are compared to abundances from Delgado Mena et al. (2010). Additional C abundances are taken from Bensby & Feltzing (2006) and additonal O abundances from Bensby et al. (2014). The abundances of the remaining elements are compared to those from Bensby et al. (2014) and Adibekyan et al. (2012b); the abundances of the latter are for stars with $T_{\rm eff}$ between 4900 and 6150 K. As can be seen in the figure, the abundances of each element of the *Kepler* planet host stars fall along the Galactic trends, demonstrating that these abundance ratios for this small subset of stars with small planets are typical of the general Galactic disk population. Generally speaking, this implies that the abundances of elements other than Fe scale with Fe in a way that is typical for similar stars in the Galactic disk.

To further demonstrate this, we show in Figures 4 and 5 the distribution of the abundances relative to solar of 13 elements for our sample of Kepler host stars excluding Kepler-68 and the sample of stars with stars with no detected planets, stars with Neptune- and super-Earth-size planets (no Jupiter-type giants), and Jupiter-type giant planets from Adibekyan et al. (2012b). We do not include Kepler-68 in these histograms, because our main interest here is to compare the compositions of stars with small planets to a general stellar population. Kepler-68 is a giant planet (Kepler-68d) host, and given that it has the highest metallicity in our sample, its inclusion would certainly skew the comparisons. Our sample of only six stars prevents us from making firm statistical conclusions based on these comparisons, but they are suggestive of possible correlations. Indeed, the histograms for the Kepler host stars, stars without known planets, and stars with Neptune- and super-Earth-size planets largely overlap, whereas the histograms for the Kepler host stars and stars with Jupiter-type giant planets appear to be offset from each other, with the latter shifted toward higher abundances.

[18]http://kepler.nasa.gov/Mission/discoveries/

To investigate these comparisons further, two-sample Kolmogorov-Smirnov (KS) tests were carried out for each element in Figures 4 and 5 for the Kepler host star sample and each of the samples of stars without known planets, stars with Neptune- and super-Earth-size planets, and stars with Jupiter-type giant planets. Again, our small sample size limits the sufficiency of the KS test to provide statistically significant probabilities of the relationships between the different samples of stars, and indeed, none of the tests yielded p-values that rejected the null hypothesis that the samples are drawn from the same parent populations. A much larger sample of detailed abundances of stars with small planets is clearly needed to determine if those abundances are in fact typical of the general Galactic disk population, and lower than those of stars with giant planets, as hinted at in Figures 4 and 5. If confirmed, this result would complement studies finding that the occurrence rate of small planets around solar-type stars and M dwarfs could be as high as 50% (e.g., Howard et al. 2012; Fressin et al. 2013; Bonfils et al. 2013; Marcy et al. 2014a; Dressing & Charbonneau 2015; Winn & Fabrycky 2015), whereas the occurrence rate of Jupiter-type giant planets around these stars is below 10% (e.g., Cumming et al. 2008; Winn & Fabrycky 2015), by suggesting that stars do not need enhanced or otherwise distinguishable chemical compositions to form small planets.

We conclude this section with a word on Li. The abundance of Li in stars with planets has been a topic of interest for some time, and there has been a debate on whether planetary hosts exhibit depleted Li abundances relative to stars without known planets for just as long. Gonzalez & Laws (2000) first suggested that stars with RV-detected planets tend to have Li abundances that are lower than field stars with detected Li based on a sample of seven planet host stars. Soon thereafter, Ryan (2000) compared the Li abundances of 16 stars with RV-detected planets to a sample of open cluster and field stars with similar ages, evolutionary states, and $T_{\rm eff}$ as the planet host stars and found that the Li abundances of the host stars are not different than those of the control sample. Subsequent to these two papers, numerous studies (e.g., Israelian et al. 2004; Takeda & Kawanomoto 2005; Sousa et al. 2010; Figueira et al. 2014; Delgado Mena et al. 2014) argue that stars with RV-detected planets do have Li abundances that are lower on average than stars without detected planets, and numerous studies (e.g., Luck & Heiter 2006; Ghezzi et al. 2010b; Meléndez et al. 2010; Ramírez et al. 2012) argue that the Li abundances of the two groups are indistinguishable. It is not clear how stars with small rocky (transiting) planets fit into this debate, because the Li abundances of a large enough sample of stars with small planets have yet been determined. Among our sample there are three stars with well-determined Li abundances and four with upper limits (Table 3). For the three stars with firm Li detections, their Li abundances are in good agreement with the general Li-$T_{\rm eff}$ trends of Ghezzi et al. (2010b) and Delgado Mena et al. (2015), and thus the Li abundances of stars with small

rocky planets do not appear to be blatantly anomalous. Li abundances of a much larger sample of stars with rocky planets are needed, though, to determine if this is actually the case.

4.3. Abundances and Condensation Temperatures

As mentioned in the Introduction, stellar abundances that correlate with T_c may indicate the presence of rocky planets. All of the *Kepler* stars in our sample are host to at least one sub-Neptune size or smaller planet, and four have at least one Earth-size planet. RV follow-up observations have, in general, only been able to place upper limits on masses of small planets except in a handful of cases, e.g., Kepler-20b, Kepler-20c, and Kepler-68b, so the densities and refractory element abundances of the majority of small planets have yet to be reliably estimated. Even with the known densities of Kepler-20b ($\rho = 6.5^{+2.0}_{-2.7}$ gcm^{-3}), Kepler-20c ($\rho = 2.91^{+0.85}_{-1.08}$ gcm^{-3}; Gautier et al. 2012), and Kepler-68b ($\rho = 3.32^{+0.86}_{-0.98}$ gcm^{-3}; Gilliland et al. 2013), the compositions are still uncertain, although densities greater than 5 gcm^{-3} are consistent with rocky and iron-nickel composition (Gautier et al. 2012; Marcy et al. 2014a,b). The upper limits on the masses for all the small planets in our sample except for Kepler-20c, Kepler-68b, and Kepler-100c allow for densities greater than 5 gcm^{-3}. Moreover, Marcy et al. (2014a) show that for the known exoplanets with 2σ mass determinations (33 planets at the time of this writing), those with radii less than 2 $R_\oplus$ have densities $\gtrsim 5$ gcm^{-3}. More recently, Rogers (2015) and Dressing et al. (2015) find that the transition from rocky to primarily non-rocky planets actually occurs at the smaller radius of 1.6 $R_\oplus$. Each of the stars in our sample, save Kepler-22, has at least one planet with a radius less than or approximately equal to 1.6 $R_\oplus$. It is therefore reasonable to assume that with the exception of Kepler-22, each star in our sample is host to at least one planet with a rocky or primarily rocky composition, and it provides a meaningful test of the T_c slope-rocky planet correlation hypothesis.

We quantify the relationship between the stellar abundances and T_c by measuring the slope of a standard least-squares fit to the refractory element ($T_c > 900$ K) abundances relative to Fe and the 50% condensation temperatures from Lodders (2003). Both unweighted fits and fits weighted by the inverse square of the total uncertainties in the [x/Fe] abundances have been made. The slopes and their 1σ uncertainties are provided in Table 8, and the weighted fits are shown in Figure 6. The difference in the slopes from the unweighted and weighted fits are statistically insignificant. Initial inspection of the fits to the data revealed that the Mn abundance falls below the fit to the [x/Fe]-T_c relation for each star, by more than the 1σ total uncertainty in the Mn abundances for three of the stars, despite the fact that

all of the Mn abundances are in agreement within uncertainties with the general Galactic population (see Figure 3). Because the T_c of Mn is 1158 K and falls near the cool end of the T_c range, these low abundances could be biasing the slopes of the fits toward more positive values. We therefore have made unweighted and weighted fits to the data with Mn removed from the list of elements; the slopes of these fits are also included in Table 8. The difference in the slopes from these unweighted and weighted fits are once again found to be statistically insignificant. Moreover, all four slope measurements for each star are consistent within the 1σ uncertainties.

The slopes for the five MS dwarfs in our sample are all positive at greater than the 2σ level, whereas the slopes for the two subgiants are negative at greater than the 1.5σ level, except for the unweighted and weighted slopes for Kepler-21 with the Mn abundance included in the calculation. In these two cases, the slopes are statistically consistent with positive values. We remind the reader that a positive slope in the [x/Fe]-T_c plane signifies an overabundance of refractory elements relative to the Sun, and in the interpretation of Meléndez et al. (2009) and Ramírez et al. (2010), suggests that the star is **not** a rocky planet host. On the other hand, a flat or negative slope signifies that the star has a similar refractory element distribution as the Sun or is deficient in refractories relative to the Sun, and thus the star would be a candidate for hosting rocky planets. Therefore, the slopes of the five MS dwarf stars are not consistent with the T_c slope-rocky planet correlation hypothesis. While the slopes for the two subgiants would appear to be consistent with the hypothesis, these stars' changing internal structure, in particular their deepening convective envelopes, have certainly mixed internal material to their surfaces, potentially changing their photospheric compositions. The T_c-planet signature is expected to be sensitive to the depth of the convective envelope during the planet formation process (e.g., Chambers 2010), so the increase in the depth of the convection zone of an evolving star could alter the signature. We therefore omit the two subgiants, Kepler-21 and Kepler-100, from the remaining discussion in this subsection.

Much of the preceding work investigating the possible correlation between T_c-abundance trends and rocky planets have focused on solar twins and analogs, and late F-type dwarfs. The former because of the similar structure to the Sun, and the latter because of the thinner convective envelopes compared to the Sun. In each case, it is thought that a planet formation signature will persist in the photospheres of these stars (e.g., Ramírez et al. 2014), as opposed to less massive stars with larger convective envelopes, in which any signature would be lost to convective mixing on a relatively short timescale. Two of the stars in our sample have convection zones that are estimated to be approximately equal to or smaller than that of the Sun, as discussed below.

The mass of Kepler-68 has been measured to be 1.079 ± 0.051 $M_\oplus$ (Gilliland et al. 2013), and thus this star would be expected to have a convective envelope that is at least similar to or thinner than that of the Sun. It is host to an Earth-size planet, a sub-Neptune, and Jupiter-type giant planet. The mass and density of the Earth-size planet, Kepler-68c, have yet to be firmly determined, but Marcy et al. (2014b) calculate upper limits of $M_\mathrm{c} \leq 2.18 \pm 3.5\ M_\oplus$ and $\rho_\mathrm{c} \leq 10.77 \pm 17.29\ \mathrm{g\,cm^{-3}}$ based on four years of RV observations. Given these upper limits and its size, it is reasonable to assume that Kepler-68c is a rocky planet. The mass and density of the sub-Neptune planet, Kepler-68b, have been determined, and at $M_\mathrm{b} = 5.97 \pm 1.7\ M_\oplus$ and $\rho_\mathrm{b} = 2.60 \pm 0.74\ \mathrm{g\,cm^{-3}}$, the planet's density falls in between those of gas giant and rocky planets. Lopez & Fortney (2014) suggest that planets like Kepler-68b represent a transition between rocky planets and gas giant planets, and may be composed of large quantities of (ice/liquid) water while lacking a large H/He gas envelope. The planetary models of Lopez & Fortney (2014) and Howe et al. (2014) suggest that if Kepler-68b has a H/He envelope at all, it makes up less than 2% of the planet mass. Using the model of Fortney et al. (2007), the composition of Kepler-68b is predicted to be close to 75% water ice and 25% rock. Assuming a 25% rocky composition for Kepler-68b and a rocky composition for Kepler-68c, a total of 3.7 $M_\oplus$ of rocky material is sequestered in these two planets. We do not include the giant planet Kepler-68d in this calculation, because it is unclear if large, gas giant planets contribute to the putative depletion of refractory elements in the host star (Schuler et al. 2011; Ramírez et al. 2014). The amount of refractory material contained in Kepler-68b and Kepler-68c is more than what has been suggested to be missing in the photosphere of the Sun, so if rocky planet formation depletes the refractory elements in host stars, we would expect to observe such a depletion in Kepler-68.

We have tested this expectation by calculating the changes in the photospheric abundances of Kepler-68 due to the extraction of 3.7 $M_\oplus$ of material from its convection zone. Using the accretion prescription of Mack et al. (2014), we calculated the abundance changes in the star assuming the accretion of 3.7 $M_\oplus$ of material and then subtracted the changes from the observed abundances to estimate the effects on the slope of the T_c-abundance relation if this amount of material had indeed been sequestered in the planets during the formation of Kepler-68b and Kepler-68c. In addition to the mass of material, the accretion model inputs include the composition of the material, the mass of the star, and the mass of the convection zone. We adopted two different compositions of the extracted material, one that matches the Earth's composition (Earth model) based on McDonough (2001) and, following Chambers (2010), one composed of 50% Earth's composition and 50% carbonaceous (CM) chondrite material (50/50 model), with the CM chondrite compositions taken from Wasson & Kallemeyn (1988). Using the mass of Kepler-68 given above, the mass of its convection zone was estimated from Figure 1 of Pinsonneault et al. (2001) using our derived

$T_{\rm eff}$. The results of the modeled abundance changes are shown in Figure 7. Both the Earth model and the 50/50 model predict abundance changes that result in slopes of the fits to the $T_{\rm c}$-abundance data that are consistent with zero. According to the $T_{\rm c}$ slope-rocky planet correlation hypothesis, a zero slope would be indicative of rocky planet formation. This result reinforces our assertion that if rocky planet formation does in fact deplete the refractory elements in host stars, we would expect to detect the signature in Kepler-68.

The second star with a convective envelope that is estimated to be roughly equal to the Sun's is Kepler-130. Density ($\rho = 0.927 \pm 0.053$ g cm^{-3}) and radius ($R = 1.127 \pm 0.033\ R_{\odot}$) estimates for Kepler-130 based on posterior distributions of stellar evolution models are presented by Rowe et al. (2014); however, these estimates are based on the stellar parameters of Huber et al. (2013), which are about 75 K and 0.11 dex in $T_{\rm eff}$ and $\log g$, respectively, lower than ours (although, as mentioned above, these are in agreement with ours within the combined uncertainty). Using their radius, density, and $\log g$, as well as our derived $\log g$, we calculate the mass of Kepler-130 to range from 0.932 $M_{\odot}$ to 1.19 $M_{\odot}$. Thus, assuming a convective envelope on par with that of the Sun's is not unreasonable. Kepler-130 is host to an Earth-size planet, a super-Earth, and a sub-Neptune; unfortunately, definitive masses have not been determined for any of them. However, the small sizes of the planets, particularly Kepler-130b ($R = 1.02 \pm 0.04\ R_{\oplus}$) and Kepler-130d ($R = 1.64 \pm 0.16\ R_{\oplus}$), are suggestive of rocky compositions. Using the empirical mass-radius relation of Weiss & Marcy (2014), we estimate the masses of the three planets to be $M_{\rm b} = 1.1\ M_{\oplus}$, $M_{\rm c} = 7.0\ M_{\oplus}$, and $M_{\rm d} = 4.3\ M_{\oplus}$ for Kepler-130b, Kepler-130c, and Kepler-130d, respectively. We then use the model of Fortney et al. (2007) to predict the compositions of the planets and find an Earth-like composition for Kepler-130b, a pure ice composition for Kepler-130c, and a pure rock composition for Kepler-130d. Considering Kepler-130b and Kepler-130d only, as much as 5.4 $M_{\oplus}$ of refractory material could be sequestered in these planets. Adopting a stellar mass of 1.061 $M_{\oplus}$ (average of the range given above) and estimating a convection zone mass using Pinsonneault et al. (2001), we use the Earth and 50/50 composition models described above to determine the effect on the slope of the $T_{\rm c}$-abundance relation if this amount of material had been sequestered in Kepler-130b and Kepler-130d. The results are shown in Figure 8. As found for Kepler-68, both the Earth model and 50/50 model predict abundance changes that result in $T_{\rm c}$-abundance slopes that are consistent with zero, suggesting that if this star's refractory elements were depleted due to small planet formation, we should be able to detect it.

One more system, Kepler-20, also warrants additional scrutiny, because masses and densities have been well determined for two of its planets (Gautier et al. 2012). The density of Kepler-20b is $\rho_{\rm b} = 6.5^{+2.0}_{-2.7}$ g cm^{-3}, placing this planet squarely in the rocky planet category, and that of Kepler-20c is $\rho_{\rm c} = 2.91^{+0.85}_{-1.08}$ g cm^{-3}, placing it in the transitional water-world

regime. Two more planets in this system, Kepler-20e and Kepler-20f, have radii near that of Earth, so it is reasonable to assume they too are rocky planets. The fifth planet in the system, Kepler-20d, has a radius equal to that of Kepler-20c within uncertainties and is probably of the water-world type planet, as well. Once again we use the empirical mass-radius relation of Weiss & Marcy (2014) to estimate the masses of Kepler-20d ($M_{\rm d} = 6.9\ M_{\oplus}$), Kepler-20e ($M_{\rm e} = 0.64\ M_{\oplus}$), and Kepler-20f ($M_{\rm f} = 1.2\ M_{\oplus}$) and the model of Fortney et al. (2007) to predict the compositions of all five planets. Compositions of the planets are found to be pure rocky for Kepler-20b, 75% water ice and 25% rocky for Kepler-20c, pure ice for Kepler-20d, and Earth-like compositions ($\sim$ 25% rocky and $\sim$ 75% iron) for both Kepler-20e and Kepler-20f. If we include only the lower limits of the masses of Kepler-20b and Kepler-20c, a total of 9.6 $M_{\oplus}$ of refractory material is contained in these two planets, whereas if we use the upper limits of the masses for these two planets and include the estimated masses of Kepler-20e and Kepler-20f, as much as 17.5 $M_{\oplus}$ of refractory material could be sequestered in these planets. The mass and radius of the host star have been estimated at $M = 0.912 \pm 0.034\ M_{\odot}$ and $R = 0.944^{+0.060}_{-0.095}\ R_{\odot}$ (Gautier et al. 2012; Fressin et al. 2012), and thus it has a larger convective envelope than the Sun. Nonetheless, using Pinsonneault et al. (2001) to estimate the mass of the star's convection zone, both the Earth and 50/50 composition models predict $T_{\rm c}$-abundance slopes that are negative or consistent with zero if either 9.6 $M_{\oplus}$ or 17.5 $M_{\oplus}$ of refractory material has been sequestered in the Kepler-20 planets (Figure 9). Once again we find that the putative rocky planet signature, if real, should be detectable in this star.

5. SUMMARY

Stellar parameters and detailed abundances of 19 elements have been derived for seven stars known to host small planets discovered by NASA's *Kepler* Mission. We have analyzed high-quality spectra obtained with the 10-m Keck telescope and HIRES echelle spectrometer as part of the *Kepler* Follow-up Observing Program and independent observations. Previously derived stellar parameters ($T_{\rm eff}$ and $\log g$) and [Fe/H] abundances by numerous other groups using automated and semi-automated routines (SME, SPC, ARES, VWA, etc.) with high-resolution spectroscopy are, in general, in good agreement with our derived values. In seven out of about 36 comparisons ($\sim$ 19%), the stellar parameters derived using automated or semi-automated routines are different than ours derived "by hand" by more than the combined uncertainties. However, in each case, the derived [Fe/H] abundances are in agreement within the uncertainties. Differences between stellar parameters and [Fe/H] abundances derived for two stars using low-resolution spectroscopic analysis and our derived values are more disparate, and while considered to be an improvement over the photometrically derived values in the *Kepler* Input Catalog, results based on low-resolution spectroscopy should be

used with caution. Our surface gravities are in good agreement with asteroseismic derived values for four of the six stars but are larger by about the 1.7σ for the other two. Nonetheless, the derived $T_{\rm eff}$ and abundances for these two stars remain robust, because they do no correlate with changes in $\log g$ and due to the small sensitivities to the $\log g$ parameter.

The metallicities of the seven stars range from [Fe/H] = -0.30 to $+0.15$, further demonstrating that small planets form around stars with both low and high metallicities (Buchhave et al. 2012; Buchhave & Latham 2015). The abundances of 15 elements are compared to those of a Galactic disk population that includes stars with and without known planets. The abundances of the *Kepler* planet host stars fall along the Galactic trends, suggesting that stars with small planets have compositions that are typical of the Galactic disk. Moreover, comparing the abundance distributions of the *Kepler* planet host stars to a sample of stars with no detected planets, a sample of Neptune- and super-Earth-size planet hosts, and a sample of Jupiter-type giant planet hosts, reveals that the former three– *Kepler* host stars, stars without known planets, and the Neptune and super-Earth-size planet hosts– may have similar compositions, whereas the *Kepler* host stars appear to have compositions that are less enhanced than those of Jupiter-type planet hosts. These results suggest that the formation of small planets does not require exceptional host-star or protoplanetary disk compositions, and that small planets may indeed be ubiquitous in the Galaxy. Our small sample size limits the statistical significance of our results, so a larger sample of stars with small planets subjected to detailed abundance analyses is needed to verify these preliminary findings.

The abundances of the refractory elements ([x/Fe]) as a function of $T_{\rm c}$ have been examined. Slopes of least-square fits to the data are found to be positive at greater than the 2σ level for the five MS dwarfs in our sample. This is contrary to expectations of the hypothesis that rocky planet formation sequesters refractory element material from host stars (Meléndez et al. 2009; Ramírez et al. 2009). Using known planet masses when available and when not, masses determined by an empirical mass-radius relation (Weiss & Marcy 2014), we make use of planet composition models (Fortney et al. 2007) to estimate the amount of refractory material contained in the rocky planets of three systems- Kepler-68, Kepler-130, and Kepler-20. In each case, we estimate that there is enough refractory material in these planets to produce an observable flat or negative trend in the [x/Fe]-$T_{\rm c}$ data if in fact small planet formation imprints such a signature on their host star. We do not see this signature for these stars.

The simplest interpretation of the positive $T_{\rm c}$ slopes we measure for these five dwarf stars known to host small planets is that there is no direct connection between the presence of small planets and depleted refractory elements in the photospheres of their host stars.

However, a definitive conclusion on the possible connection between the presence of rocky planets and the detailed composition of a stellar atmosphere cannot be made based solely on our modest sample size, but our results do indicate that there is not a simple correlation between the two. The first suggestion that rocky planet formation may affect the refractory element abundances of the host star resulted from a fine analysis of the Sun (Meléndez et al. 2009), the planetary architecture of which is unlike any of the stars in our sample. Our stars all have planets with semimajor axes smaller than that of Mercury, with the exception of the sub-Neptune Kepler-22b ($a = 0.85$ AU Borucki et al. 2012) and the giant planet Kepler-68d ($a = 1.4$ AU Gilliland et al. 2013), so the architecture of a planetary system may play an important role. Also, factors such as stellar age, stellar structure, Galactic chemical evolution, and stellar birthplace in the Galaxy could all affect the composition of a star (Ramírez et al. 2014; Adibekyan et al. 2014; Nissen 2015). The planet formation process is undoubtedly complex, and determining if small planet formation in particular alters the compositions of the host stars has revealed itself to be quite challenging. Detailed abundance analyses of stars known to host small planets offer the best way to resolve the current discordance in the field, and with the *Kepler* mission successfully identifying numerous small planets, such analyses are now possible.

Finally, the seeming lack of dependence of small planet formation on metallicity and the concomitant propensity of giant planets to form around metal-rich stars are characteristic of core accretion models of planet formation (e.g., Ida & Lin 2004), as demonstrated by planet population syntheses (e.g., Mordasini et al. 2012). The core accretion paradigm is the most widely accepted model of planet formation, but many details still need to be worked out (e.g., Ida et al. 2013; Fortier et al. 2013) if a single model is to explain the observed properties of the known planetary systems. Furthermore, the competing paradigm of planet formation, gravitational instability (e.g., Boss 1997), may yet play a role in any unified theory of planet formation (e.g., Forgan & Rice 2013). The continued characterization of planetary systems, including the detailed compositions of host stars, will be necessary to guide future efforts in fashioning such a theory.

We graciously thank F. Valdes at NOAO for his help with the processing of the Keck/HIRES data, as well as G. Marcy and A. Howard for their role in obtaining the FOP/Keck spectra. S.C.S. acknowledges support provided by grant NNX12AD19G from the National Aeronautics and Space Administration as part of the Kepler Participating Scientist Program. Some data presented herein were obtained at the W. M. Keck Observatory from telescope time allocated to the National Aeronautics and Space Administration through the agency's scientific partnership with the California Institute of Technology and the University of California. The Observatory was made possible by the generous financial support of the W. M. Keck

Foundation. Additional data were obtained at Kitt Peak National Observatory, National Optical Astronomy Observatory, which is operated by the Association of Universities for Research in Astronomy (AURA) under cooperative agreement with the National Science Foundation. This research has made use of the NASA Exoplanet Archive, which is operated by the California Institute of Technology, under contract with the National Aeronautics and Space Administration under the Exoplanet Exploration Program.

Facilities: Keck:I (HIRES) KPNO:4.0m (Echelle)

A. Appendix

Three different group members measured EWs for three separate sets of stars in our sample, and in order to ensure as much consistency as possible in the final relative abundances, each person also measured EWs in the solar spectrum appropriate for each star. The measured EWs and resulting absolute abundances for each line of all elements for each star are provided in Table 9, and the three sets of solar EWs and absolute abundances are provided in Table 10.

REFERENCES

Adibekyan, V. Z., Delgado Mena, E., Sousa, S. G., et al. 2012a, A&A, 547, A36

Adibekyan, V. Z., González Hernández, J. I., Delgado Mena, E., et al. 2014, A&A, 564, L15

Adibekyan, V. Z., Sousa, S. G., Santos, N. C., et al. 2012, A&A, 545, A32

Allende Prieto, C., Lambert, D. L., & Asplund, M. 2001, ApJ, 556, L63

Asplund, M., Grevesse, N., Sauval, A. J., Allende Prieto, C., & Blomme, R. 2005, A&A, 431, 693

Barclay, T., Rowe, J. F., Lissauer, J. J., et al. 2013, Nature, 494, 452

Batalha, N. M., Rowe, J. F., Bryson, S. T., et al. 2013, ApJS, 204, 24

Bensby, T., & Feltzing, S. 2006, MNRAS, 367, 1181

Bensby, T., Feltzing, S., & Oey, M. S. 2014, A&A, 562, A71

Bonfils, X., Delfosse, X., Udry, S., et al. 2013, A&A, 549, A109

Borucki, W. J., Koch, D. G., Basri, G., et al. 2011, ApJ, 736, 19

Borucki, W. J., Koch, D. G., Batalha, N., et al. 2012, ApJ, 745, 120

Boss, A. P. 1997, Science, 276, 1836

Brown, T. M., Latham, D. W., Everett, M. E., & Esquerdo, G. A. 2011, AJ, 142, 112

Bruntt, H., Catala, C., Garrido, R., et al. 2002, A&A, 389, 345

Bruntt, H., Basu, S., Smalley, B., et al. 2012, MNRAS, 423, 122

Bubar, E. J., & King, J. R. 2010, AJ, 140, 293

Buchhave, L. A., & Latham, D. W. 2015, ApJ, 808, 187

Buchhave, L. A., Latham, D. W., Johansen, A., et al. 2012, Nature, 486, 375

Buchhave, L. A., Bizzarro, M., Latham, D. W., et al. 2014, Nature, 509, 593

Cabrera, J., Csizmadia, S., Lehmann, H., et al. 2014, ApJ, 781, 18

Casagrande, L., Schönrich, R., Asplund, M., et al. 2011, A&A, 530, A138

Chambers, J. E. 2010, ApJ, 724, 92

Chaplin, W. J., & Miglio, A. 2013, ARA&A, 51, 353

Chaplin, W. J., Basu, S., Huber, D., et al. 2014, ApJS, 210, 1

Cumming, A., Butler, R. P., Marcy, G. W., et al. 2008, PASP, 120, 531

Delgado Mena, E., Israelian, G., González Hernández, J. I., et al. 2010, ApJ, 725, 2349

—. 2014, A&A, 562, A92

Delgado Mena, E., Bertrán de Lis, S., Adibekyan, V. Z., et al. 2015, A&A, 576, A69

Doyle, L. R., Carter, J. A., Fabrycky, D. C., et al. 2011, Science, 333, 1602

Dressing, C. D., & Charbonneau, D. 2015, ApJ, 807, 45

Dressing, C. D., Charbonneau, D., Dumusque, X., et al. 2015, ApJ, 800, 135

Everett, M. E., Howell, S. B., Silva, D. R., & Szkody, P. 2013, ApJ, 771, 107

Fabbian, D., Asplund, M., Barklem, P. S., Carlsson, M., & Kiselman, D. 2009, A&A, 500, 1221

Figueira, P., Faria, J. P., Delgado-Mena, E., et al. 2014, A&A, 570, A21

Fischer, D. A., & Valenti, J. 2005, ApJ, 622, 1102

Fitzpatrick, M. J., & Sneden, C. 1987, in Bulletin of the American Astronomical Society, Vol. 19, Bulletin of the American Astronomical Society, 1129–+

Forgan, D., & Rice, K. 2013, MNRAS, 432, 3168

Fortier, A., Alibert, Y., Carron, F., Benz, W., & Dittkrist, K.-M. 2013, A&A, 549, A44

Fortney, J. J., Marley, M. S., & Barnes, J. W. 2007, ApJ, 659, 1661

Frasca, A., Alcalá, J. M., Covino, E., et al. 2003, A&A, 405, 149

Fressin, F., Torres, G., Rowe, J. F., et al. 2012, Nature, 482, 195

Fressin, F., Torres, G., Charbonneau, D., et al. 2013, ApJ, 766, 81

Gaidos, E. 2015, ApJ, 804, 40

Gautier, III, T. N., Charbonneau, D., Rowe, J. F., et al. 2012, ApJ, 749, 15

Ghezzi, L., Cunha, K., Smith, V. V., et al. 2010a, ApJ, 720, 1290

Ghezzi, L., Cunha, K., Smith, V. V., & de la Reza, R. 2010b, ApJ, 724, 154

Gilliland, R. L., Marcy, G. W., Rowe, J. F., et al. 2013, ApJ, 766, 40

Gonzalez, G., & Laws, C. 2000, AJ, 119, 390

González Hernández, J. I., Delgado-Mena, E., Sousa, S. G., et al. 2013, A&A, 552, A6

González Hernández, J. I., Israelian, G., Santos, N. C., et al. 2010, ApJ, 720, 1592

Howard, A. W., Marcy, G. W., Bryson, S. T., et al. 2012, ApJS, 201, 15

Howe, A. R., Burrows, A., & Verne, W. 2014, ApJ, 787, 173

Howell, S. B., Rowe, J. F., Bryson, S. T., et al. 2012, ApJ, 746, 123

Huber, D., Chaplin, W. J., Christensen-Dalsgaard, J., et al. 2013, ApJ, 767, 127

Huber, D., Silva Aguirre, V., Matthews, J. M., et al. 2014, ApJS, 211, 2

Ida, S., & Lin, D. N. C. 2004, ApJ, 616, 567

Ida, S., Lin, D. N. C., & Nagasawa, M. 2013, ApJ, 775, 42

Israelian, G., Santos, N. C., Mayor, M., & Rebolo, R. 2004, A&A, 414, 601

Israelian, G., Delgado Mena, E., Santos, N. C., et al. 2009, Nature, 462, 189

Johansson, S., Litzén, U., Lundberg, H., & Zhang, Z. 2003, ApJ, 584, L107

Johns-Krull, C. M., McCullough, P. R., Burke, C. J., et al. 2008, ApJ, 677, 657

Johnson, J. A., Ivans, I. I., & Stetson, P. B. 2006, ApJ, 640, 801

Kalas, P., Graham, J. R., Chiang, E., et al. 2008, Science, 322, 1345

King, J. R., Deliyannis, C. P., Hiltgen, D. D., et al. 1997, AJ, 113, 1871

Kiselman, D. 1991, A&A, 245, L9

Kupka, F., Piskunov, N., Ryabchikova, T. A., Stempels, H. C., & Weiss, W. W. 1999, A&AS, 138, 119

Kupka, F. G., Ryabchikova, T. A., Piskunov, N. E., Stempels, H. C., & Weiss, W. W. 2000, Baltic Astronomy, 9, 590

Lissauer, J. J., Marcy, G. W., Bryson, S. T., et al. 2014, ApJ, 784, 44

Lodders, K. 2003, ApJ, 591, 1220

Lopez, E. D., & Fortney, J. J. 2014, ApJ, 792, 1

Luck, R. E., & Heiter, U. 2006, AJ, 131, 3069

Mack, III, C. E., Schuler, S. C., Stassun, K. G., & Norris, J. 2014, ApJ, 787, 98

Maldonado, J., Eiroa, C., Villaver, E., Montesinos, B., & Mora, A. 2015, A&A, 579, A20

Marcy, G. W., & Butler, R. P. 1992, PASP, 104, 270

Marcy, G. W., Weiss, L. M., Petigura, E. A., et al. 2014a, Proceedings of the National Academy of Science, 111, 12655

Marcy, G. W., Butler, R. P., Vogt, S. S., et al. 2008, Physica Scripta Volume T, 130, 014001

Marcy, G. W., Isaacson, H., Howard, A. W., et al. 2014b, ApJS, 210, 20

Mathur, S., Metcalfe, T. S., Woitaszek, M., et al. 2012, ApJ, 749, 152

McDonough, W. 2001, in Earthquake Thermodynamics and Phase Transitions in the Earth's Interior, ed. R. Teisseyre & E. Majewski, Vol. 76 (Academic Press, San Diego), 3–23

Meléndez, J., Asplund, M., Gustafsson, B., & Yong, D. 2009, ApJ, 704, L66

Meléndez, J., Ramírez, I., Casagrande, L., et al. 2010, Ap&SS, 328, 193

Meléndez, J., Bergemann, M., Cohen, J. G., et al. 2012, A&A, 543, A29

Molenda-Żakowicz, J., Sousa, S. G., Frasca, A., et al. 2013, MNRAS, 434, 1422

Mordasini, C., Alibert, Y., Benz, W., Klahr, H., & Henning, T. 2012, A&A, 541, A97

Mortier, A., Sousa, S. G., Adibekyan, V. Z., Brandão, I. M., & Santos, N. C. 2014, A&A, 572, A95

Nissen, P. E. 2015, A&A, 579, A52

Önehag, A., Gustafsson, B., & Korn, A. 2014, A&A, 562, A102

Önehag, A., Korn, A., Gustafsson, B., Stempels, E., & Vandenberg, D. A. 2011, A&A, 528, A85

Pinsonneault, M. H., DePoy, D. L., & Coffee, M. 2001, ApJ, 556, L59

Piskunov, N. E., Kupka, F., Ryabchikova, T. A., Weiss, W. W., & Jeffery, C. S. 1995, A&AS, 112, 525

Prochaska, J. X., & McWilliam, A. 2000, ApJ, 537, L57

Ramírez, I., Allende Prieto, C., & Lambert, D. L. 2013, ApJ, 764, 78

Ramírez, I., Asplund, M., Baumann, P., Meléndez, J., & Bensby, T. 2010, A&A, 521, A33+

Ramírez, I., Fish, J. R., Lambert, D. L., & Allende Prieto, C. 2012, ApJ, 756, 46

Ramírez, I., Meléndez, J., & Asplund, M. 2009, A&A, 508, L17

—. 2014, A&A, 561, A7

Ramírez, I., Khanal, S., Aleo, P., et al. 2015, ApJ, 808, 13

Rogers, L. A. 2015, ApJ, 801, 41

Rowe, J. F., Bryson, S. T., Marcy, G. W., et al. 2014, ApJ, 784, 45

Ryabchikova, T. A., Piskunov, N. E., Kupka, F., & Weiss, W. W. 1997, Baltic Astronomy, 6, 244

Ryan, S. G. 2000, MNRAS, 316, L35

Sanchis-Ojeda, R., Rappaport, S., Winn, J. N., et al. 2013, ApJ, 774, 54

Santos, N. C., Israelian, G., & Mayor, M. 2001, A&A, 373, 1019

Santos, N. C., Adibekyan, V., Mordasini, C., et al. 2015, A&A, 580, L13

Schaeuble, M., & King, J. R. 2012, PASP, 124, 164

Schlaufman, K. C. 2015, ApJ, 799, L26

Schuler, S. C., Flateau, D., Cunha, K., et al. 2011, ApJ, 732, 55

Schuler, S. C., King, J. R., Fischer, D. A., Soderblom, D. R., & Jones, B. F. 2003, AJ, 125, 2085

Schuler, S. C., King, J. R., Hobbs, L. M., & Pinsonneault, M. H. 2004, ApJ, 602, L117

Schuler, S. C., King, J. R., Terndrup, D. M., et al. 2006, ApJ, 636, 432

Schuler, S. C., Plunkett, A. L., King, J. R., & Pinsonneault, M. H. 2010, PASP, 122, 766

Silva Aguirre, V., Casagrande, L., Basu, S., et al. 2012, ApJ, 757, 99

Silva Aguirre, V., Davies, G. R., Basu, S., et al. 2015, MNRAS, 452, 2127

Sneden, C. 1973, ApJ, 184, 839

Sousa, S. G., Fernandes, J., Israelian, G., & Santos, N. C. 2010, A&A, 512, L5

Sousa, S. G., Santos, N. C., Israelian, G., Mayor, M., & Monteiro, M. J. P. F. G. 2007, A&A, 469, 783

Sousa, S. G., Santos, N. C., Mayor, M., et al. 2008, A&A, 487, 373

Takeda, Y. 2003, A&A, 402, 343

Takeda, Y., & Honda, S. 2005, PASJ, 57, 65

Takeda, Y., & Kawanomoto, S. 2005, PASJ, 57, 45

Teske, J. K., Cunha, K., Schuler, S. C., Griffith, C. A., & Smith, V. V. 2013, ApJ, 778, 132

Torres, G., Fischer, D. A., Sozzetti, A., et al. 2012, ApJ, 757, 161

Udry, S., Mayor, M., Benz, W., et al. 2006, A&A, 447, 361

Valenti, J. A., & Piskunov, N. 1996, A&AS, 118, 595

Vogt, S. S., Allen, S. L., Bigelow, B. C., et al. 1994, in Society of Photo-Optical Instrumentation Engineers (SPIE) Conference Series, Vol. 2198, Society of Photo-Optical Instrumentation Engineers (SPIE) Conference Series, ed. D. L. Crawford & E. R. Craine, 362

Wang, J., & Fischer, D. A. 2015, AJ, 149, 14

Wasson, J. T., & Kallemeyn, G. W. 1988, Philosophical Transactions of the Royal Society of London Series A, 325, 535

Weiss, L. M., & Marcy, G. W. 2014, ApJ, 783, L6

Winn, J. N., & Fabrycky, D. C. 2015, ARA&A, 53, 409

Yong, D., Lambert, D. L., Allende Prieto, C., & Paulson, D. B. 2004, ApJ, 603, 697

This preprint was prepared with the AAS LaTeX macros v5.2.

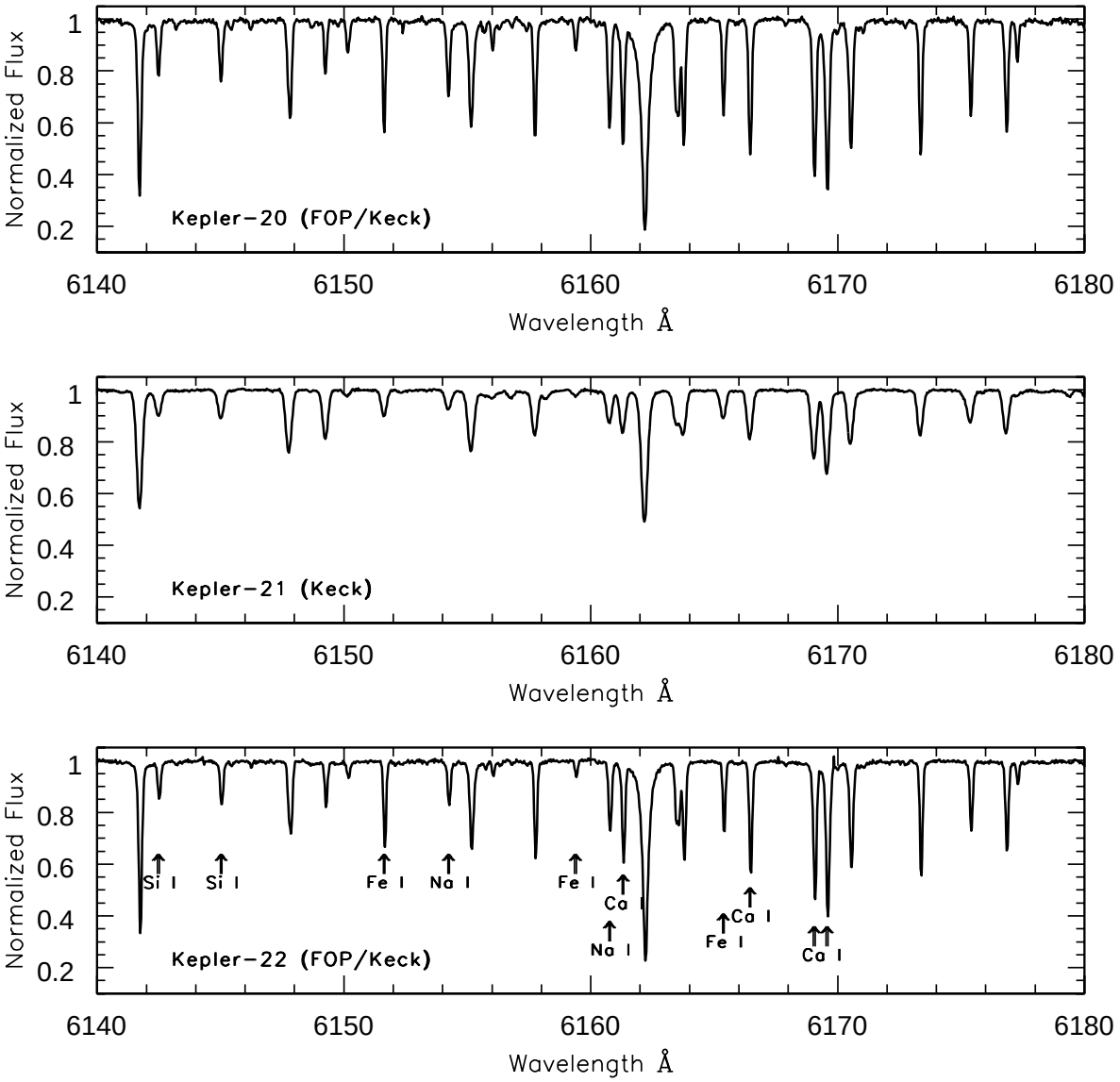

Fig. 1.— Sample Keck/HIRES spectra of some of the *Kepler* stars. Lines for which EWs were measured are marked.

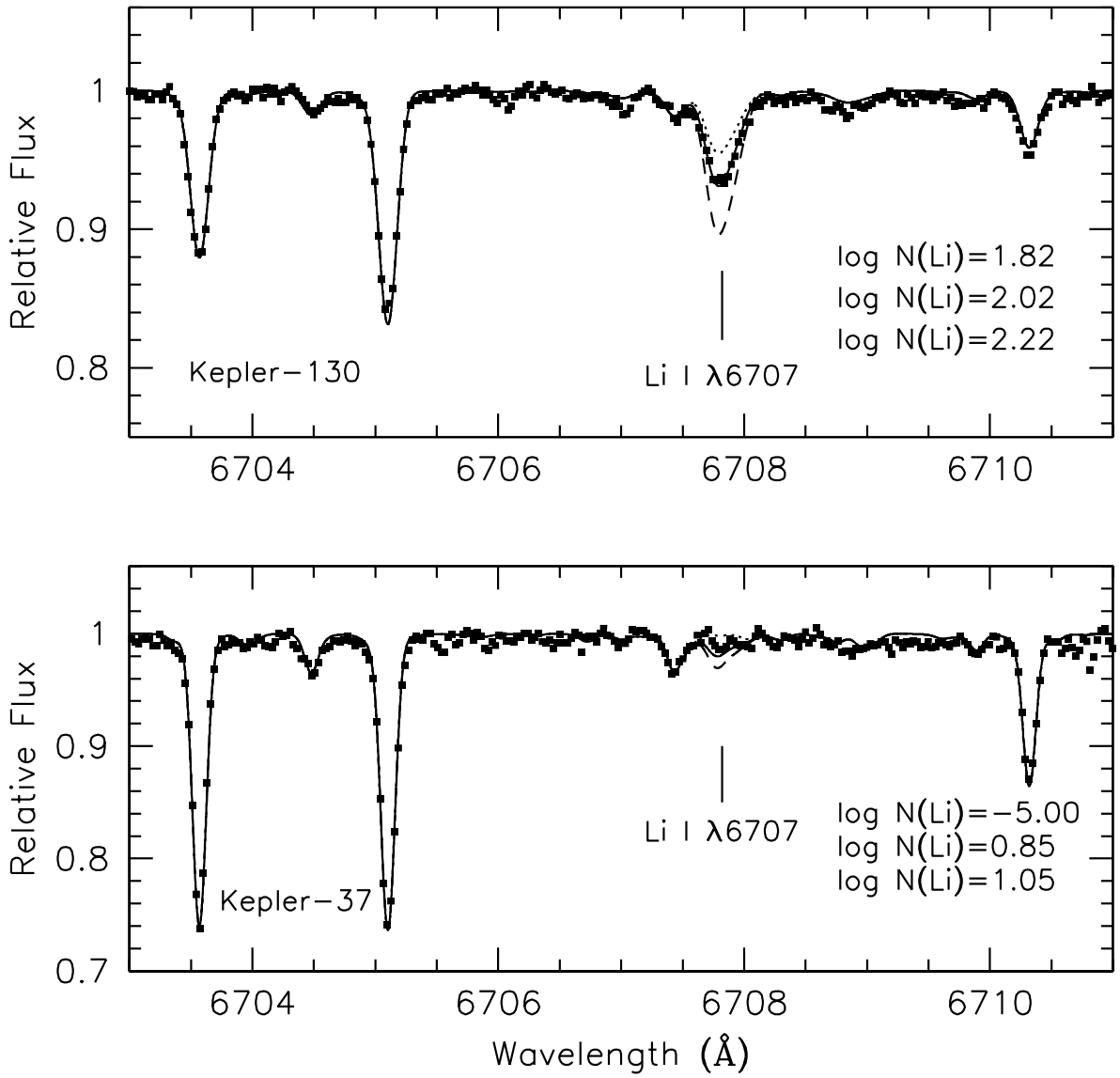

Fig. 2.— Observed spectra (points) and synthetic fits (lines) of the λ6707 Li I region of Kepler-37 (bottom panel) and Kepler-130 (top panel). Syntheses are shown for three input Li abundances for each star. For Kepler-130, the best fit abundance and $\pm$0.20 dex around the best fit abundance are shown. In the case of Kepler-37, for which a definitive Li measurement was not possible, syntheses for no Li, an upper limit on the Li abundance, and 0.20 dex larger than the upper limit are provided.

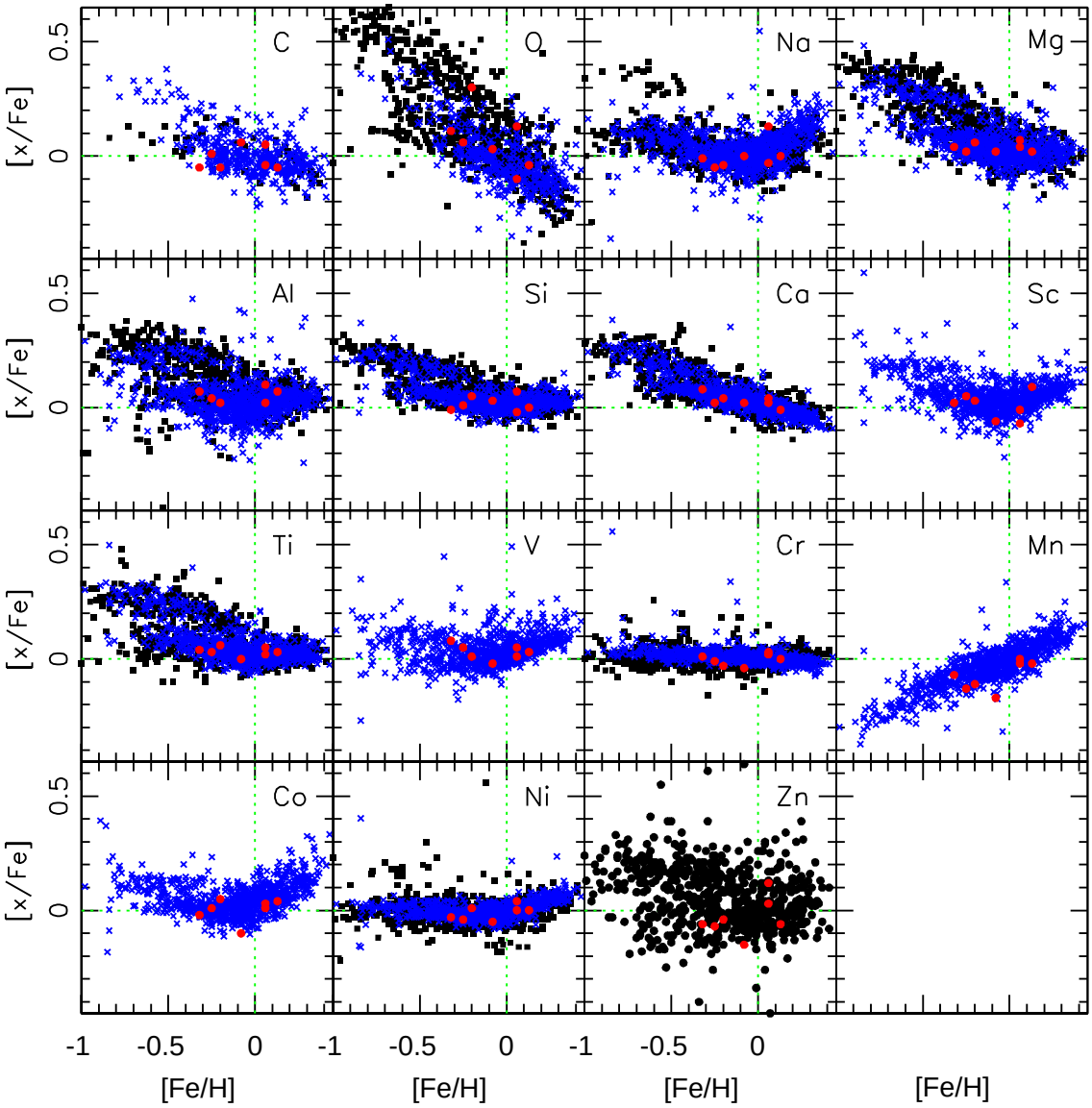

Fig. 3.— [x/Fe] ratios as a function of [Fe/H]. The red circles are the *Kepler* stars. For C and O, the blue crosses are abundances taken from Delgado Mena et al. (2010); black squares are from Bensby & Feltzing (2006) and the large sample of Bensby et al. (2014), repspectively. For the remaining elements, blue crosses are from Adibekyan et al. (2012b), and black squares are from Bensby et al. (2014). Solar values are indicated by the green dotted lines.

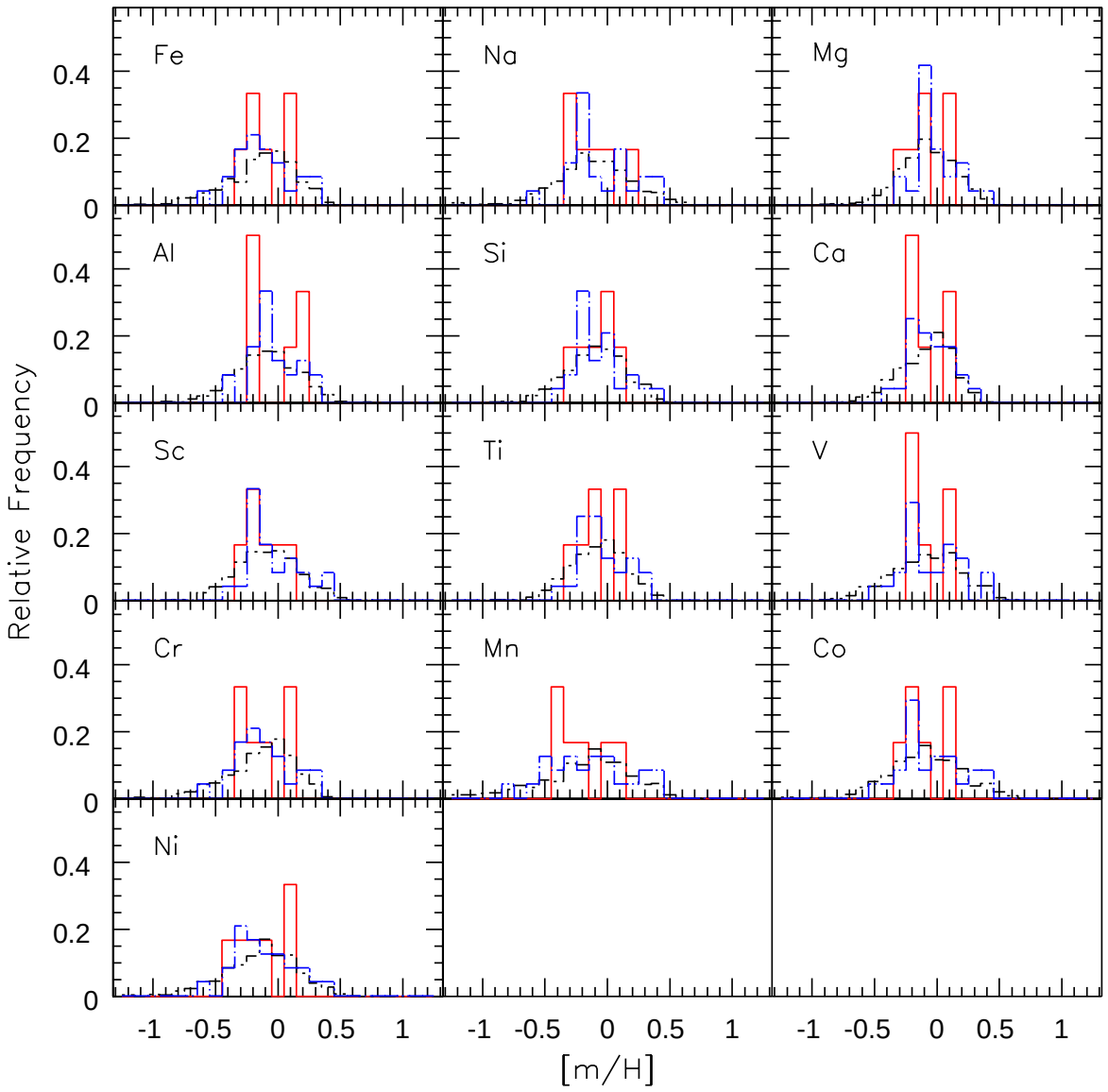

Fig. 4.— Comparison between abundances of the Kepler host stars (red solid lines) and those of stars without known planets (black dot-dash lines) and stars with Neptune- and super-Earth-size planets (blue dot-dash lines). The data for the stars without known planets and with Neptune- and super-Earth-size planets are from Adibekyan et al. (2012b). There is significant overlap of all three histograms for each element.

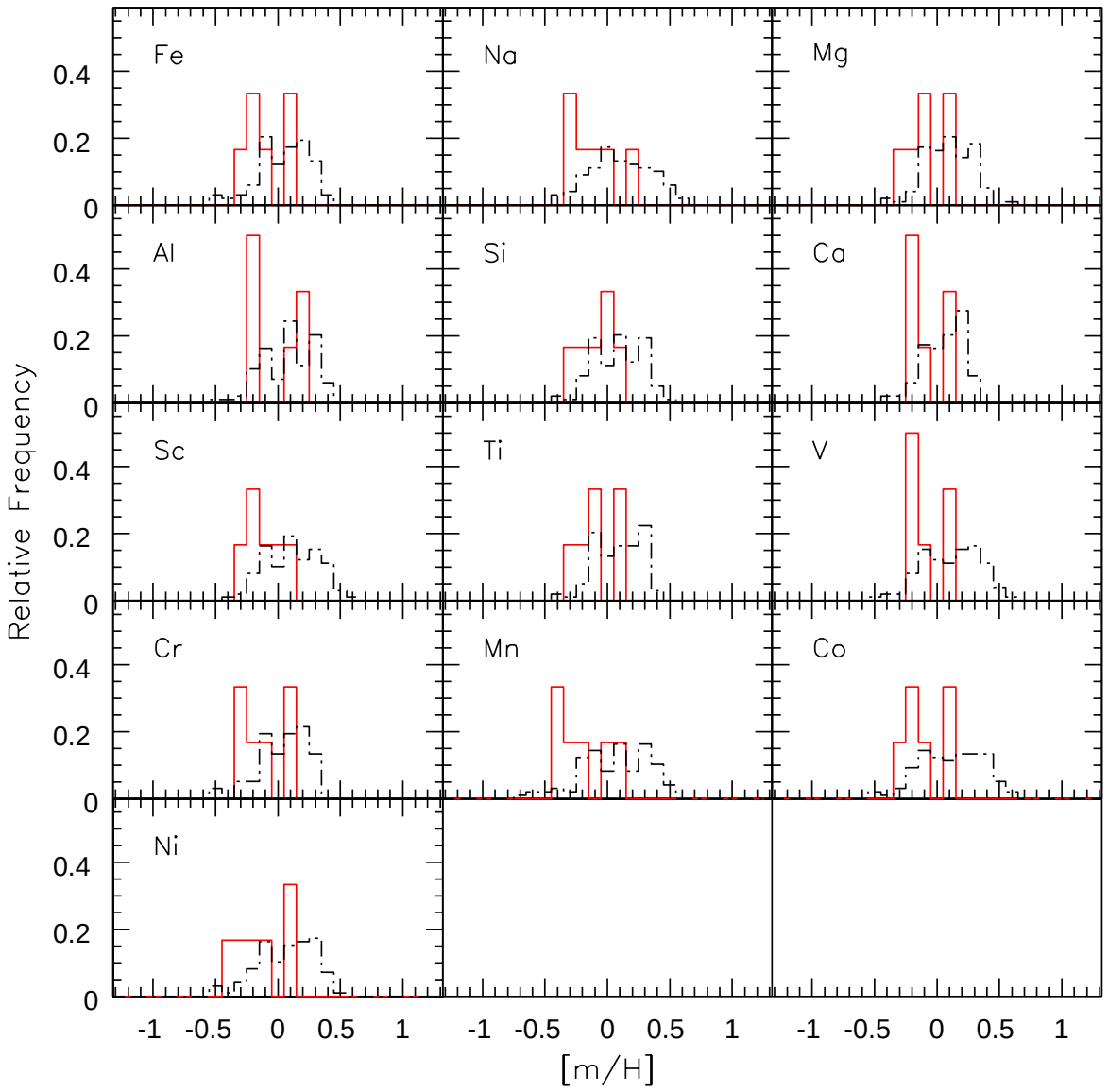

Fig. 5.— Comparison between abundances of the Kepler host stars (red solid lines) and those of stars with Jupiter-type giant planets (black dot-dash lines). The data for the stars with Jupiter-type giant planets are from Adibekyan et al. (2012b). Despite the small sample of Kepler host stars, there appears to be an offset between the two samples, with the Jupiter-type planet hosts shifted to higher abundances.

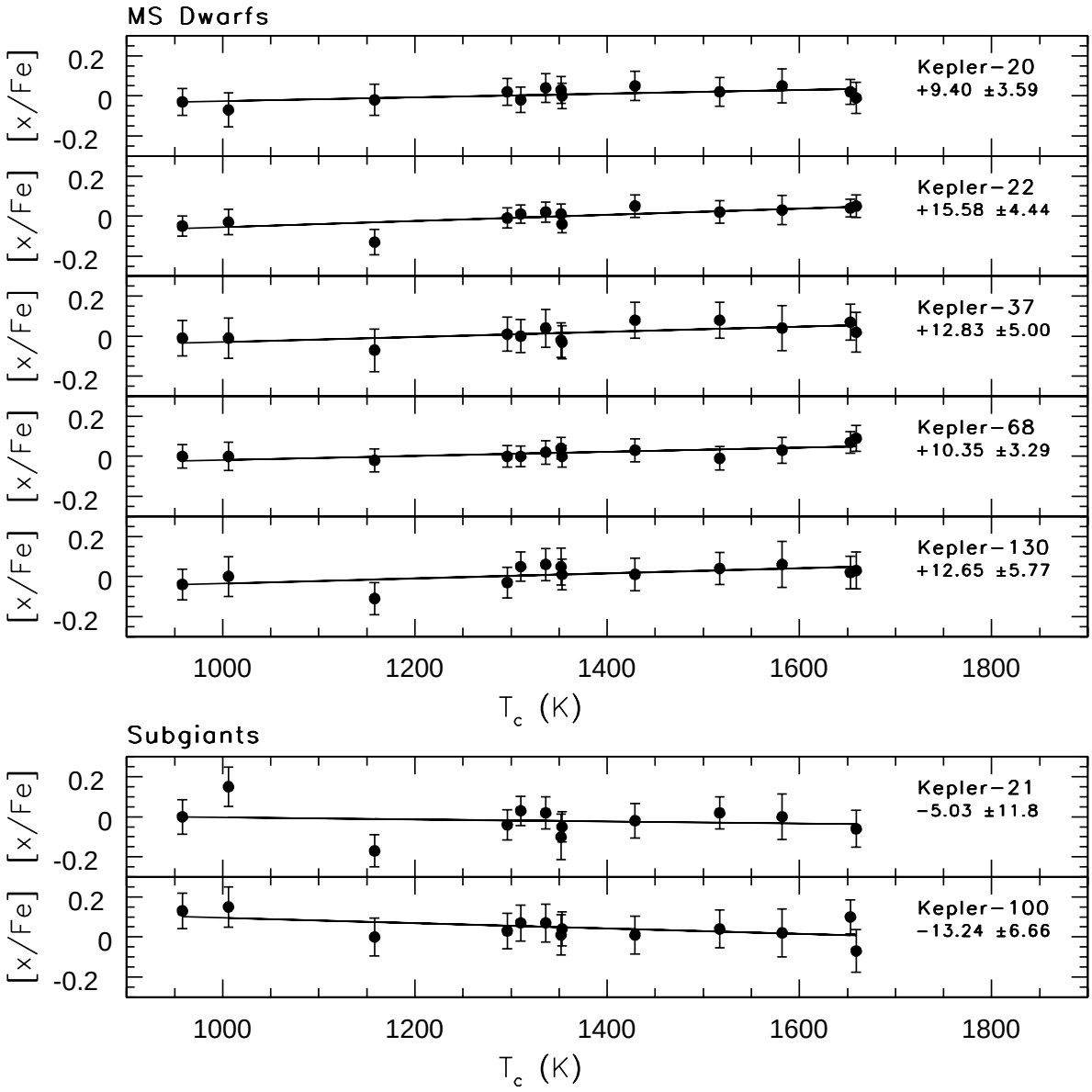

Fig. 6.— Abundances versus condensation temperature of the elements. The solid line is a linear least-squares fit to the data weighted by the inverse square of the total uncertainty in each abundance. The MS dwarfs are displayed in the top group, and the subgiants are shown in the bottom group. The slope and uncertainty of the fit are also provided, in units of $\times 10^{-5}$ dex K^{-1}

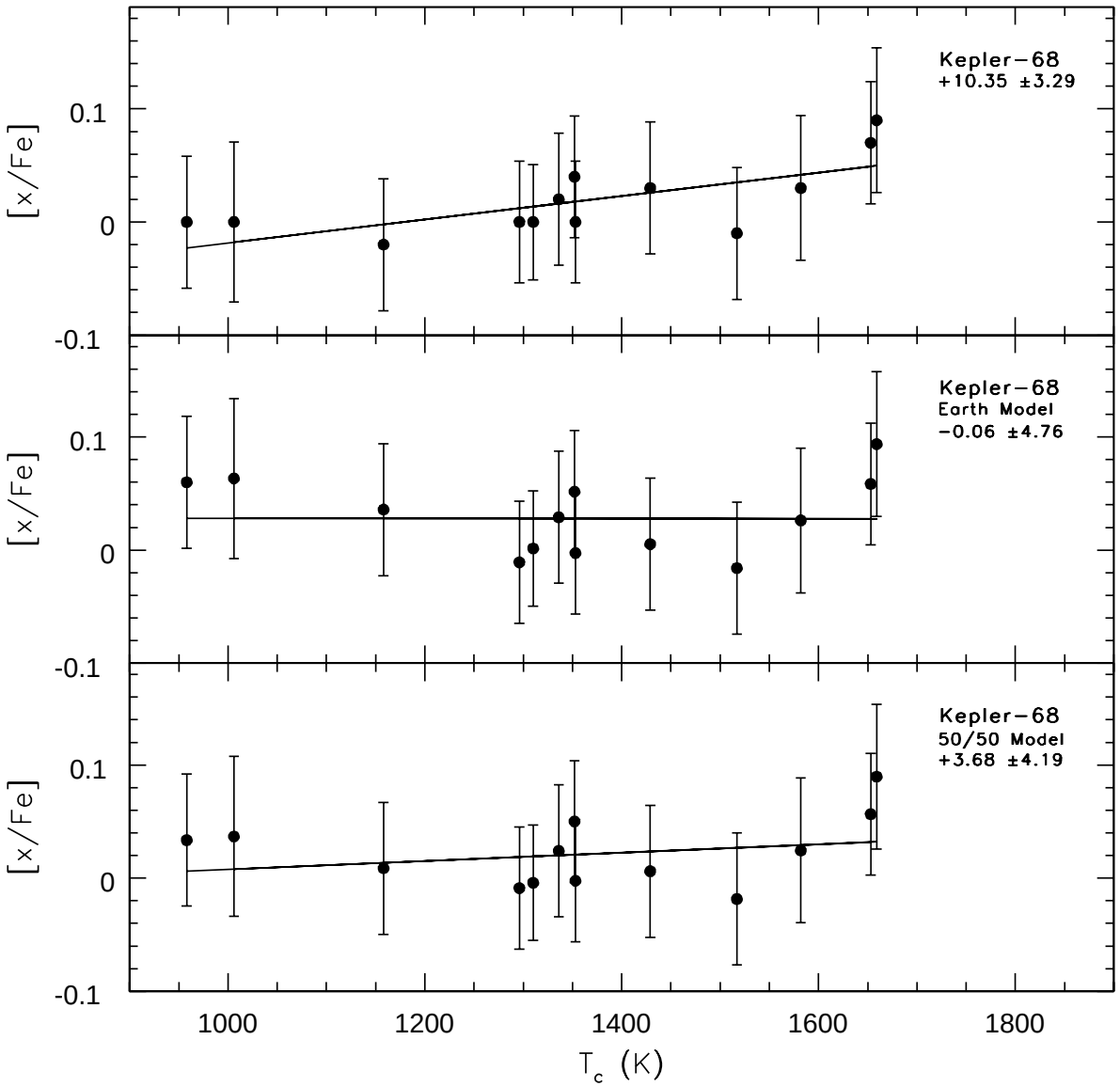

Fig. 7.— Abundances versus condensation temperature of the elements for Kepler-68. The top panel shows the derived abundances, which are identical to those in Figure 6. The middle panel shows the modeled abundances after removing 3.7 $M_\oplus$ of material with Earth-like composition, and the bottom panel shows the modeled abundances after removing the same amount of material composed of 50% Earth-like composition and 50% CM chondrite composition, as described in the text. The solid lines are the linear least-squares fits to the data weighted by the inverse square of the total uncertainty in each abundance. The slope and uncertainty of the fit are also provided, in units of $\times 10^{-5}$ dex K^{-1}. For both cases of the modeled abundances, the resulting slopes of the least-squares fits are negative or consistent with zero, which would be in concordance with the T_c slope-rocky planet correlation hypothesis, if real.

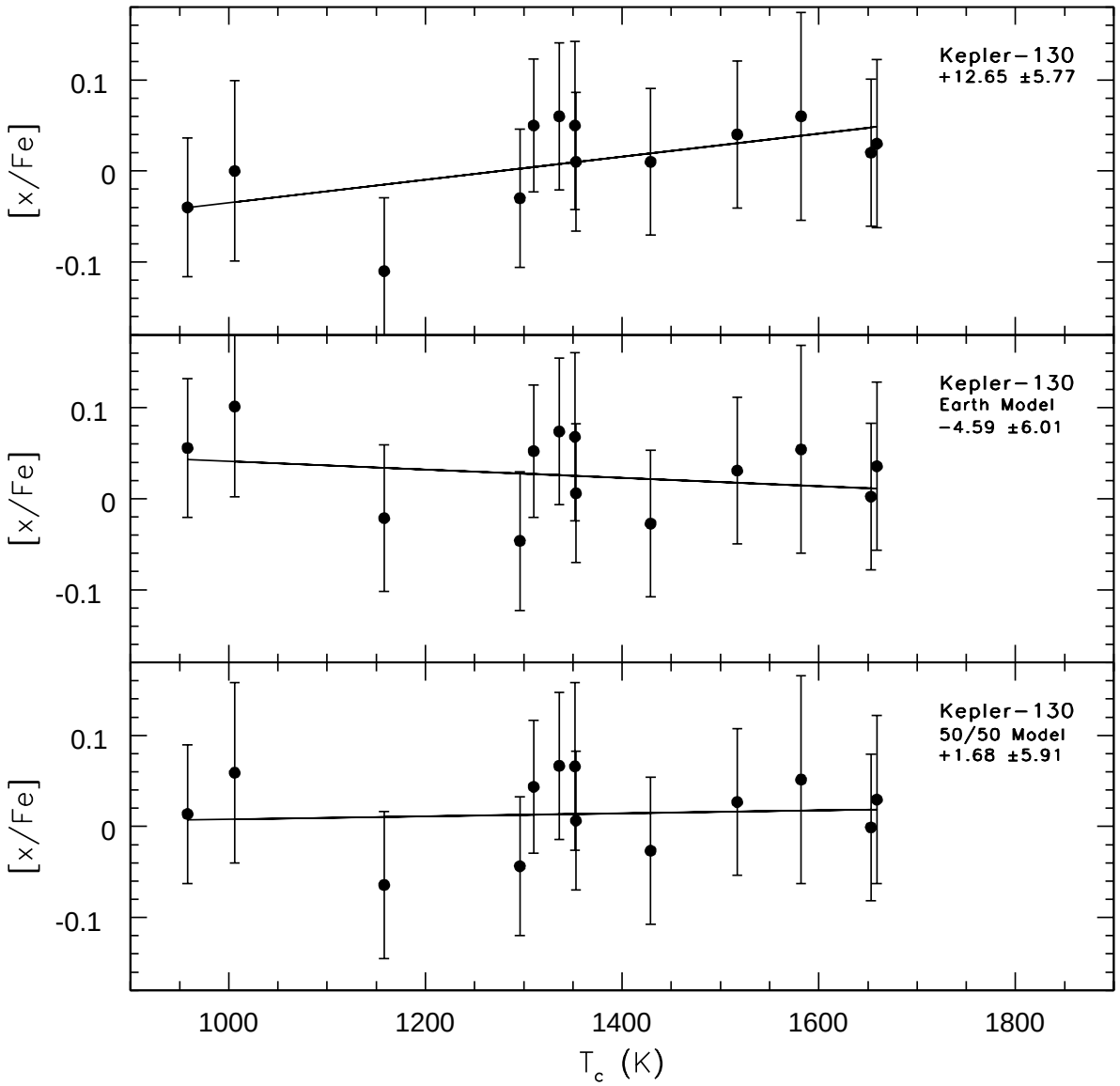

Fig. 8.— Abundances versus condensation temperature of the elements for Kepler-130. The top panel shows the derived abundances, which are identical to those in Figure 6. The middle panel shows the modeled abundances after removing 5.4 $M_\oplus$ of material with Earth-like composition, and the bottom panel shows the modeled abundances after removing the same amount of material composed of 50% Earth-like composition and 50% CM chondrite composition, as described in the text. The solid lines are the linear least-squares fits to the data weighted by the inverse square of the total uncertainty in each abundance. The slope and uncertainty of the fit are also provided, in units of $\times 10^{-5}$ dex K^{-1}. For both cases of the modeled abundances, the resulting slopes of the least-squares fits are negative or consistent with zero, which would be in concordance with the T_c slope-rocky planet correlation hypothesis, if real.

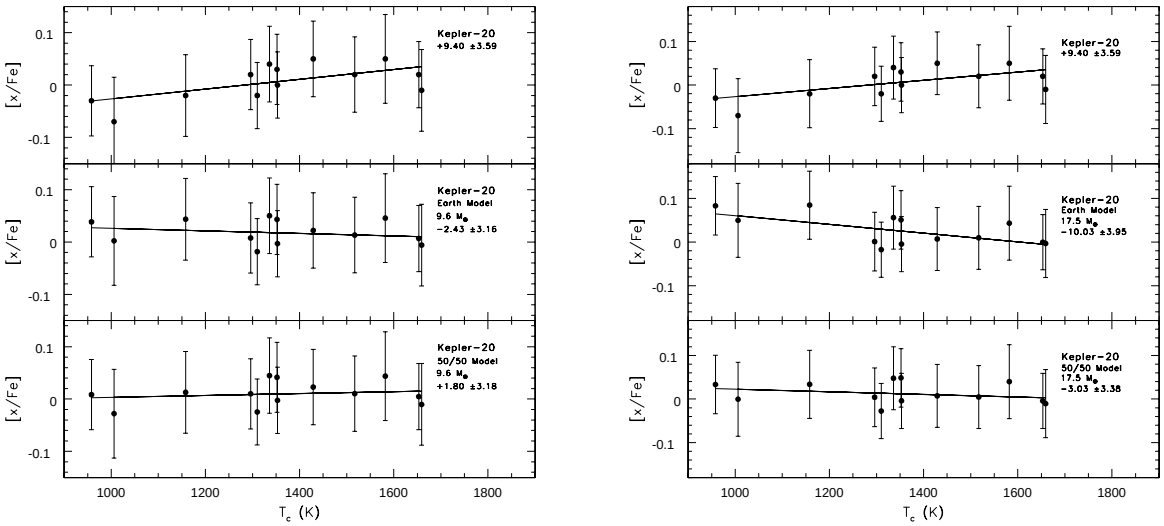

Fig. 9.— Abundances versus condensation temperature of the elements for Kepler-20. The top panels show the derived abundances, which are identical to those in Figure 6. The middle panels show the modeled abundances after removing 9.6 $M_\oplus$ (left) and 17.5 $M_\oplus$ (right) of material with Earth-like composition, and the bottom panels show the modeled abundances after removing the same amount of material composed of 50% Earth-like composition and 50% CM chondrite composition, as described in the text. The solid lines are the linear least-squares fits to the data weighted by the inverse square of the total uncertainty in each abundance. The slope and uncertainty of the fit are also provided, in units of $\times 10^{-5}$ dex K^{-1}. For all cases of the modeled abundances, the resulting slopes of the least-squares fits are negative or consistent with zero, which would be in concordance with the T_c slope-rocky planet correlation hypothesis, if real.

Table 1. Observing Log

Star	KOI	KIC	K_p [a]	Date (UT)	S/N [b]	Comment
Kepler-20	70	6850504	12.5	2010 Aug 24	231	FOP/Keck
Kepler-21	975	3632418	8.2	2011 Jul 12	482[c]	Keck
				2010 Sep 01	160	FOP/Keck
				2011 Apr 19	435	KPNO
Kepler-22	87	10593626	11.7	2010 Sep 25	314[d]	FOP/Keck
				2011 Sep 05		FOP/Keck
Kepler-37	245	8478994	9.7	2010 Aug 02	258	FOP/Keck
Kepler-68	246	11295426	10.0	2010 Aug 02	250	FOP/Keck
Kepler-100	41	6521045	11.0	2012 Aug 31	340	Keck
Kepler-130	282	5088536	11.5	2012 Aug 31	290	Keck

[a]Borucki et al. (2011)

[b]S/N estimates given at 6700 Å

[c]S/N at 6850 Å

[d]S/N of combined FOP/Keck sepctra

Table 2. Stellar Parameters

Star	$T_{\rm eff}$ (K)	$\log g$ (cgs)	ξ (km s^{-1})	[Fe I/H]	N	σ_μ	[Fe II/H]	N	σ_μ	Comment
Kepler-20	5514±25	4.44±0.12	1.15±0.04	+0.059	61	0.003	+0.062	13	0.009	FOP/Keck
Kepler-21	6177±42	3.99±0.15	1.98±0.15	-0.079	48	0.006	-0.079	13	0.011	Keck
	6125±45	3.90±0.18	1.95±0.16	-0.102	46	0.006	-0.096	14	0.012	FOP/Keck
	6240±45	4.18±0.14	1.82±0.20	-0.057	44	0.007	-0.060	5	0.017	KPNO
Kepler-22	5622±30	4.57±0.08	1.47±0.12	-0.251	61	0.004	-0.250	14	0.012	FOP/Keck
Kepler-37	5406±28	4.49±0.13	1.36±0.06	-0.323	58	0.004	-0.321	13	0.020	FOP/Keck
Kepler-68	5887±28	4.45±0.10	1.57±0.05	+0.126	65	0.004	+0.131	14	0.024	FOP/Keck
Kepler-100	5855±40	3.98±0.15	1.49±0.06	+0.061	41	0.005	+0.063	11	0.015	Keck
Kepler-130	5958±37	4.41±0.15	1.78±0.11	-0.199	49	0.005	-0.195	11	0.022	Keck

Table 3. Abundances

Element	Kepler-20	Kepler-21	Kepler-22	Kepler-37	Kepler-68	Kepler-100	Kepler-130
$\log N$(Li)	< 1.10	< 1.20	< 1.00	< 0.85	2.05 ±0.09	2.21 ±0.08	2.02 ±0.08
[C/H]	+0.02±0.06	-0.02±0.05	-0.24±0.05	-0.37±0.03	+0.08±0.05	+0.11±0.08	-0.25±0.07
[O/H]	-0.04±0.08	-0.05±0.07	-0.19±0.05	-0.21±0.07	+0.09±0.04	+0.19±0.10	+0.10±0.09
[Na/H]	+0.03±0.03	-0.08±0.05	-0.30±0.03	-0.33±0.04	+0.13±0.03	+0.19±0.04	-0.24±0.03
[Mg/H]	+0.10±0.04	-0.06±0.04	-0.23±0.03	-0.28±0.05	+0.15±0.03	+0.13±0.05	-0.14±0.04
[Al/H]	+0.08±0.02	···	-0.21±0.02	-0.25±0.04	+0.20±0.02	+0.16±0.03	-0.18±0.04
[Si/H]	+0.04±0.02	-0.05±0.02	-0.24±0.02	-0.32±0.02	+0.13±0.01	+0.13±0.04	-0.15±0.02
[S/H]	···	-0.13±0.05	···	-0.37±0.03	+0.11±0.04	+0.11±0.06	-0.33±0.05
[K/H]	-0.01±0.06	+0.07±0.07	-0.28±0.05	-0.33±0.06	+0.13±0.05	+0.21±0.06	-0.20±0.07
[Ca/H]	+0.08±0.04	-0.06±0.04	-0.23±0.04	-0.24±0.04	+0.12±0.03	+0.10±0.05	-0.16±0.04
[Sc/H]	+0.05±0.05	-0.14±0.06	-0.20±0.04	-0.30±0.06	+0.22±0.05	-0.01±0.07	-0.17±0.06
[Ti/H]	+0.11±0.06	-0.08±0.09	-0.22±0.06	-0.28±0.08	+0.16±0.04	+0.08±0.09	-0.14±0.09
[V/H]	+0.11±0.04	-0.10±0.05	-0.20±0.04	-0.24±0.04	+0.16±0.03	+0.07±0.05	-0.19±0.04
[Cr/H]	+0.08±0.03	-0.12±0.03	-0.26±0.03	-0.31±0.03	+0.13±0.02	+0.09±0.04	-0.23±0.03
[Mn/H]	+0.04±0.05	-0.25±0.04	-0.38±0.05	-0.39±0.07	+0.11±0.03	+0.06±0.05	-0.31±0.04
[Fe/H]	+0.06±0.06	-0.08±0.07	-0.25±0.04	-0.32±0.08	+0.13±0.05	+0.06±0.08	-0.20±0.07
[Co/H]	+0.09±0.03	-0.18±0.09	-0.24±0.03	-0.34±0.03	+0.17±0.02	+0.07±0.06	-0.15±0.06
[Ni/H]	+0.06±0.02	-0.13±0.03	-0.29±0.02	-0.35±0.02	+0.13±0.02	+0.10±0.03	-0.19±0.03
[Zn/H]	+0.09±0.02	-0.23±0.05	-0.32±0.03	-0.38±0.03	+0.07±0.02	+0.18±0.05	-0.24±0.04

Table 4. Carbon Abundances

Star	[C I/H]	σ	[C_2/H]	σ	<[C/H]>[a]	N	σ_μ
Kepler-20	+0.01	0.03	+0.04	0.01	+0.02	5	0.01
Kepler-21	-0.02	0.02	···	···	-0.02	4	0.01
Kepler-22	-0.23	0.02	-0.26	0.01	-0.24	6	0.01
Kepler-37	-0.21	0.09	-0.37	0.01	-0.37	2	0.01
Kepler-68	+0.08	0.03	+0.10	0.02	+0.08	6	0.01
Kepler-100	+0.14	0.07	+0.05	0.02	+0.11	6	0.03
Kepler-130	-0.24	0.01	-0.28	0.04	-0.25	6	0.01

[a]Final adopted abundance.

Table 5. Oxygen Abundances

Star	[O I]	O I Triplet				[O/H][a]
	[O/H]	$[O/H]_{LTE}$	σ	$[O/H]_{NLTE}$	σ	
Kepler-20	-0.04	-0.03	0.02	-0.01	0.02	-0.04
Kepler-21	-0.05	+0.15	0.03	0.00	0.00	-0.05
Kepler-22	···	-0.21	0.02	-0.19	0.02	-0.19
Kepler-37	-0.21	-0.28	0.02	···	···	-0.21
Kepler-68	···	+0.12	0.01	+0.09	0.00	+0.09
Kepler-100	···	+0.29	0.11	+0.19	0.08	+0.19
Kepler-130	···	+0.14	0.08	+0.10	0.07	+0.10

[a]Final adopted abundance.

Table 6. Abundance Sensitivities

Species	Kepler-20			Kepler-21			Kepler-22		
	$\Delta T_{\rm eff}$ ($\pm$150 K)	$\Delta \log g$ ($\pm$0.25 dex)	$\Delta\xi$ ($\pm$0.30kms^{-1})	$\Delta T_{\rm eff}$ ($\pm$150 K)	$\Delta \log g$ ($\pm$0.25 dex)	$\Delta\xi$ ($\pm$0.30kms^{-1})	$\Delta T_{\rm eff}$ ($\pm$150 K)	$\Delta \log g$ ($\pm$0.25 dex)	$\Delta\xi$ ($\pm$0.30kms^{-1})
Fe I	$\pm$0.09	$\pm$0.01	$\mp$0.05	$\pm$0.10	$\pm$0.01	$\mp$0.02	$\pm$0.01	$\pm$0.09	$\mp$0.02
Fe II	$^{-0.07}_{+0.10}$	$^{+0.13}_{-0.10}$	$\mp$0.05	$\mp$0.02	$\pm$0.10	$\mp$0.05	$\pm$0.11	$\mp$0.06	$\mp$0.03
C I	$^{-0.09}_{+0.13}$	$^{+0.10}_{-0.07}$	$\mp$0.01	$\mp$0.08	$\pm$0.09	$\mp$0.01	$\mp$0.10	$\pm$0.09	$\mp$0.01
O I	$^{-0.15}_{+0.19}$	$^{+0.09}_{-0.05}$	$\mp$0.02	$\mp$0.11	$\pm$0.07	$\mp$0.05	$\mp$0.15	$\pm$0.08	$\mp$0.02
Na I	$\pm$0.10	$\mp$0.05	$\mp$0.03	$\pm$0.07	$\mp$0.02	$\mp$0.02	$\pm$0.09	$\mp$0.03	$\mp$0.02
Mg I	$\pm$0.07	$\mp$0.03	$^{-0.09}_{+0.05}$	$\pm$0.07	$\mp$0.02	$\mp$0.03	$\pm$0.08	$\mp$0.03	$\mp$0.02
Al I	$\pm$0.08	$\mp$0.02	$\mp$0.02	...	...	...	$\pm$0.08	$\mp$0.01	$\mp$0.01
Si I	$\pm$0.02	$\pm$0.02	$\mp$0.02	$\pm$0.05	$\mp$0.01	$\mp$0.02	$\pm$0.01	$\pm$0.02	$\mp$0.01
S I	$^{-0.06}_{+0.09}$	$^{+0.10}_{-0.07}$	$\mp$0.01	$\mp$0.04	$\pm$0.08	$\mp$0.01	...	...	...
K I	$\pm$0.14	$^{-0.12}_{+0.09}$	$^{-0.07}_{+0.04}$	$\pm$0.13	$\mp$0.06	$\mp$0.12	$\pm$0.15	$\mp$0.10	$\mp$0.07
Ca I	$\pm$0.13	$\mp$0.06	$\mp$0.06	$\pm$0.10	$\mp$0.03	$\mp$0.05	$\pm$0.12	$\mp$0.04	$\mp$0.04
Sc II	$\mp$0.01	$\pm$0.11	$\mp$0.02	$\pm$0.03	$\pm$0.10	$\mp$0.02	0.00	$\pm$0.11	$\mp$0.01
Ti I	$\pm$0.18	$\mp$0.03	$\mp$0.10	$\pm$0.14	$\mp$0.02	$\mp$0.03	$\pm$0.17	$\mp$0.02	$\mp$0.06
Ti II	$\mp$0.01	$\pm$0.09	$\mp$0.10	$\pm$0.02	$\pm$0.10	$\mp$0.10	$\mp$0.01	$\pm$0.10	$\mp$0.07
V I	$\pm$0.18	$\mp$0.01	$\mp$0.04	$\pm$0.14	$\mp$0.02	$\mp$0.01	$\pm$0.18	$\mp$0.01	$\mp$0.01
Cr I	$\pm$0.11	$\mp$0.03	$\mp$0.05	$\pm$0.10	$\mp$0.01	$\mp$0.02	$\pm$0.11	$\mp$0.02	$\mp$0.03
Mn I	$\pm$0.16	$\mp$0.03	$\mp$0.11	$\pm$0.14	$\mp$0.02	$\mp$0.01	$\pm$0.15	$\mp$0.01	$\mp$0.03
Co I	$\pm$0.11	$\pm$0.03	$\mp$0.02	$\pm$0.13	$\mp$0.02	$\mp$0.01	$\pm$0.11	$\pm$0.03	$\mp$0.01
Ni I	$\pm$0.07	$\pm$0.02	$\mp$0.05	$\pm$0.10	$\mp$0.01	$\mp$0.02	$\pm$0.08	$\pm$0.02	$\mp$0.03
Zn I	$\pm$0.01	$^{+0.03}_{+0.03}$	$\mp$0.11	$\pm$0.08	$\pm$0.02	$\mp$0.10	0.00	$\pm$0.05	$\mp$0.07

Table 7. Comparison of Stellar Parameters

Star	$T_{\rm eff}$	$\log g$	[Fe/H]	Method	Reference	Comment
Kepler-20	5514±25	4.44±0.12	+0.06±0.06	MOOG	this study	
	5455±100	4.4±0.1	+0.01±0.04	SME	Gautier et al. (2012)	
	5466±93	4.443±0.075	+0.02±0.04	SME	Fressin et al. (2012)	
	5547±50	4.55±0.10	+0.04±0.08	SPC	Buchhave et al. (2014)	
Kepler-21	6177±42	3.99±0.15	-0.08±0.07	MOOG	this study	
	6131±44	4.0±0.1	-0.15±0.06	Multiple	Howell et al. (2012)	1
	6148±111	3.94±0.21	-0.19±0.21	ROTFIT*	Molenda-Żakowicz et al. (2013)	2
	6409±74	4.43±0.12	-0.03±0.06	ARES/MOOG	Molenda-Żakowicz et al. (2013)	
	5928±75	3.25±0.15	-0.20±0.10	spec fit	Everett et al. (2013)	3
	6190±60	4.00±0.03	-0.16±0.06	VWA	Bruntt et al. (2012)	
	6123±50	3.86±0.10	-0.20±0.08	SPC	Buchhave et al. (2014)	7
	6286±70	$4.018^{+0.003}_{-0.004}$	-0.01	Astero	Silva Aguirre et al. (2012)	4
	6305±50	4.026±0.04	-0.03±0.10	Astero	Silva Aguirre et al. (2015)	5
	6120±70	4.01±0.01	-0.17±0.07	Astero	Mathur et al. (2012)	6
	5838±178	$4.008^{+0.011}_{-0.031}$	-0.20±0.30	Astero	Chaplin et al. (2014)	7
	6190±84	$4.010^{+0.010}_{-0.009}$	-0.16±0.09	Astero	Chaplin et al. (2014)	8
Kepler-22	5622±30	4.57±0.08	-0.25±0.04	MOOG	this study	
	5518±44	4.44±0.06	-0.29±0.06	SME	Borucki et al. (2012)	
	5642±50	4.49±0.10	-0.27±0.08	Multiple	Borucki et al. (2012)	9
	5626±50	4.54±0.10	-0.23±0.08	SPC	Buchhave et al. (2014)	
	5642±50	4.443±0.027	-0.27±0.08	Astero	Huber et al. (2014)	10
Kepler-37	5406±28	4.49±0.13	-0.32±0.08	MOOG	this study	
	5417±75	4.5667±0.0065	-0.32±0.07	Mulitple	Barclay et al. (2013)	11
	5442±50	4.52±0.10	-0.33±0.08	SPC	Buchhave et al. (2012)	
	5430±50	4.61±0.10	-0.34±0.08	SPC	Buchhave et al. (2014)	
	5241±75	4.33±0.15	-0.55±0.10	spec fit	Everett et al. (2013)	3

Table 7—Continued

Star	$T_{\rm eff}$	$\log g$	[Fe/H]	Method	Reference	Comment
Kepler-68	5887±28	4.45±0.10	+0.13±0.05	MOOG	this study	
	5793±74	4.281±0.06	+0.12±0.074	Multiple	Gilliland et al. (2013)	12
	5758±50	4.21±0.10	+0.07±0.08	SPC	Buchhave et al. (2012)	
	5777±50	4.21±0.10	+0.04±0.08	SPC	Buchhave et al. (2014)	
	5793±74	4.280±0.003	+0.12±0.07	Astero	Silva Aguirre et al. (2015)	13
Kepler-100	5855±40	3.98±0.15	+0.06±0.08	MOOG	this study	
	5909	4.30	···	SME	Batalha et al. (2013)	14
	5825±75	4.125±0.03	+0.02±0.10	Multiple	Marcy et al. (2014b)	15
	5798±49	4.09±0.10	+0.03±0.08	SPC	Buchhave et al. (2012)	
	5824±49	4.13±0.10	+0.07±0.08	SPC	Buchhave et al. (2014)	
	5825±75	4.125±0.004	+0.02±0.10	Astero	Silva Aguirre et al. (2015)	16
Kepler-130	5958±37	4.41±0.15	-0.20±0.07	MOOG	this study	
	5884±75	4.304±0.053	-0.22±0.010	Multiple	Huber et al. (2013)	17
	5873±50	4.29±0.10	-0.22±0.08	SPC	Buchhave et al. (2012)	
	5861±50	4.29±0.10	-0.15±0.08	SPC	Buchhave et al. (2014)	

[1]Howell et al. (2012) used multiple sources to estimate the adopted parameters.

[2]The ROTFIT package is described in Frasca et al. (2003).

[3]The authors developed a spectrum fitting routine catered to low-resolution spectroscopy.

[4]The [Fe/H] for the asteroseismic analysis is taken from Casagrande et al. (2011). The $T_{\rm eff}$ is determined in an iterative fashion using the infrared flux method (IRFM). See Silva Aguirre et al. (2012) for details.

[5][Fe/H] and $T_{\rm eff}$ are derived using a high-resolution spectrum obtained from the *Kepler* Community Follow-up Observing Program (CFOP). See Silva Aguirre et al. (2015) for details.

[6][Fe/H] and $T_{\rm eff}$ are those of the optimal model from the Asteroseismic Modeling Portal; while the corresponding uncertainties are those reported for the spectroscopically derived values. The uncertainty in $\log g$ is the quadratic sum of the uncertainties in the derived radius and mass.

[7][Fe/H] and $T_{\rm eff}$ are field-average values and determined using the IRFM, respectively. See Chaplin et al. (2014) for details.

[8][Fe/H] and $T_{\rm eff}$ adopted from Bruntt et al. (2012).

[9]Stellar parameters are derived from five separate spectra using various spectrum fitting techniques. See Borucki et al. (2012) for details.

[10][Fe/H] and $T_{\rm eff}$ are taken from Borucki et al. (2012).

[11]SME and SPC were used to analyze two different spectra obtained with two different telescopes. The initial set of parameters and metallicity were used as input for an asteroseismic analysis to determine $\log g$. [Fe/H] and $T_{\rm eff}$ were then rederived while holding the $\log g$ fixed at the asteroseismic value. See Barclay et al. (2013) for details.

[12]An initial set of parameters and metallicity were derived using SME and then used as input for an asteroseismic analysis to determine $\log g$. [Fe/H] and $T_{\rm eff}$ were then rederived while holding the $\log g$ fixed at the asteroseismic value. See Gilliland et al. (2013) for details.

[13][Fe/H] and $T_{\rm eff}$ are taken from Gilliland et al. (2013).

[14]Uncertainties in $T_{\rm eff}$ and $\log g$ are not provided, and no [Fe/H] is reported.

[15]An initial set of parameters and metallicity were derived using SME and then used as input for an asteroseismic analysis to determine $\log g$. [Fe/H] and $T_{\rm eff}$ were then rederived while holding the $\log g$ fixed at the asteroseismic value. See for Marcy et al. (2014b) details.

[16][Fe/H] and $T_{\rm eff}$ are taken from Marcy et al. (2014b).

[17]An initial set of parameters and metallicity were derived using SME or SPC (which is not specified) and then used as input for an asteroseismic analysis to determine $\log g$. [Fe/H] and $T_{\rm eff}$ were then rederived while holding the $\log g$ fixed at the asteroseismic value. See for Huber et al. (2013) details.

Table 8. Abundance Slopes with T_c

	Unweighted Slope[a]				Weighted Slope			
Star	w/Mn	σ	w/o Mn	σ	w/Mn	σ	w/o Mn	σ
Kepler-20	+10.27	3.67	+10.03	3.98	+9.40	3.59	+9.12	3.88
Kepler-21	-8.11	11.4	-14.85	8.78	-5.03	11.8	-13.23	8.57
Kepler-22	+16.41	4.75	+12.70	2.69	+15.58	4.44	+12.89	2.98
Kepler-37	+12.74	4.84	+10.40	4.47	+12.83	5.00	+11.02	4.81
Kepler-68	+10.06	3.18	+9.30	3.34	+10.35	3.29	+9.57	3.49
Kepler-100	-15.25	6.51	-18.22	6.15	-13.24	6.66	-16.10	6.34
Kepler-130	+12.19	5.48	+8.39	3.90	+12.65	5.77	+8.64	4.17

[a]all slopes are $\times 10^{-5}$ dex K^{-1}

Table 9. Lines Measured, Equivalent Widths, and Abundances

	λ	χ		Kepler-20		Kepler-21		Kepler-22		Kepler-37		Kepler-68		Kepler-100		Kepler-130	
Ion	(Å)	(eV)	log gf	EW	log N	EW	log N	EW	log N	EW	log N	EW	log N	EW	log N	EW	log N
C I	5052.17	7.68	-1.304	26.1	8.45	52.5	8.41	16.6	8.17	12.9	8.13	39.8	8.51	45.9	8.51	27.9	8.23
	5380.34	7.68	-1.615	14.6	8.44	34.0	8.42	10.7	8.27	8.4	8.25	27.1	8.58	33.2	8.59	15.1	8.20
	6587.61	8.54	-1.021	8.7	8.36	26.0	8.38	7.2	8.26	···	···	20.5	8.56	26.4	8.61	10.5	8.16
	7111.47	8.64	-1.074	···	···	19.0	8.34	···	···	···	···	14.4	8.51	13.8	8.36	8.7	8.21
	7113.18	8.65	-0.762	···	···	···	···	14.1	8.45	11.2	8.47	30.5	8.66	36.9	8.69	14.7	8.18
O I	6300.30[a]	0.00	-9.720	6.6	8.64	5.1	8.63	···	···	4.5	8.47	···	···	···	···	···	···
	7771.94	9.15	0.369	51.0	8.81	124.9	9.03	47.4	8.64	33.8	8.56	83.9	8.93	104.9	9.17	89.6	8.92
	7774.17	9.15	0.223	47.1	8.88	115.5	9.06	43.2	8.71	28.8	8.57	76.8	8.98	94.8	9.17	88.8	9.06
	7775.39	9.15	0.001	31.7	8.76	85.4	8.89	26.8	8.57	17.2	8.44	54.7	8.85	59.8	8.84	54.0	8.76
Na I	5682.63	2.10	-0.700	112.2	6.31	81.3	6.27	82.6	5.95	93.1	5.96	111.3	6.47	110.5	6.60	77.3	6.10
	6154.23	2.10	-1.560	47.7	6.32	23.0	6.21	27.2	6.02	29.7	5.96	40.7	6.40	41.2	6.42	19.5	6.02
	6160.75	2.10	-1.260	69.9	6.34	35.5	6.16	43.9	6.01	48.9	5.97	62.5	6.41	60.3	6.41	34.1	6.03
Mg I	4730.03	4.35	-2.523	88.0	7.98	52.0	7.80	58.5	7.60	62.7	7.54	75.7	7.98	61.7	7.83	43.0	7.56
	5711.09	4.35	-1.833	119.8	7.67	83.8	7.52	98.9	7.39	106.3	7.36	113.7	7.76	102.0	7.71	67.3	7.46
	6965.41	5.75	-1.510	32.7	7.37	···	···	18.9	7.14	15.9	7.00	32.5	7.46	···	···	···	···
Al I	6696.02	3.14	-1.347	50.2	6.34	···	···	30.6	6.05	32.4	5.98	47.2	6.46	42.5	6.40	23.6	6.07
	6698.67	3.14	-1.647	29.5	6.29	···	···	16.3	6.02	18.1	5.97	26.8	6.40	25.2	6.38	12.1	6.03
Si I	5690.43	4.93	-1.769	53.7	7.53	38.6	7.38	37.6	7.23	33.5	7.13	57.1	7.61	53.0	7.53	36.4	7.28
	5701.10	4.93	-1.581	41.2	7.13	29.8	7.03	27.2	6.85	26.6	6.81	45.7	7.25	···	···	···	···
	5708.40	4.95	-1.034	77.8	7.17	67.6	7.10	61.3	6.87	59.0	6.81	81.8	7.24	···	···	···	···
	5772.15	5.08	-1.358	56.0	7.29	44.6	7.20	38.2	6.97	34.0	6.88	59.6	7.37	···	···	···	···
	6125.02	5.61	-1.464	34.3	7.52	26.7	7.44	23.4	7.28	18.6	7.15	39.8	7.63	38.7	7.60	21.4	7.27
	6142.48	5.62	-1.295	36.9	7.40	30.2	7.34	24.3	7.13	20.0	7.02	38.8	7.45	35.8	7.38	22.4	7.13
	6145.02	5.62	-1.310	39.5	7.45	30.3	7.36	27.9	7.22	21.9	7.08	44.9	7.55	43.5	7.52	26.8	7.24
	6243.81	5.62	-1.242	50.5	7.56	41.8	7.49	34.4	7.27	28.1	7.14	54.1	7.62	61.2	7.73	36.5	7.35
	6244.47	5.62	-1.093	47.6	7.37	39.4	7.30	32.1	7.08	27.4	6.98	50.5	7.42	54.5	7.48	34.2	7.16
	6414.98	5.87	-1.035	50.1	7.54	40.2	7.46	33.0	7.25	27.9	7.16	53.4	7.59	53.4	7.61	36.8	7.36
	6741.63	5.98	-1.428	17.0	7.42	···	···	11.9	7.23	8.0	7.04	19.6	7.50	19.3	7.46	11.3	7.23
	6848.58	5.86	-1.524	20.7	7.51	13.5	7.34	···	···	11.9	7.21	24.2	7.60	19.5	7.46	11.6	7.23
	7003.57	5.96	-0.937	61.1	7.67	52.6	7.61	42.4	7.38	38.5	7.32	65.7	7.72	···	···	···	···
	7405.77	5.61	-0.313	90.8	7.14	83.5	7.10	74.6	6.86	72.9	6.84	98.1	7.21	···	···	···	···
S I	4694.11	6.53	-1.770	···	···	···	···	···	···	···	···	16.7	7.50	15.4	7.32	5.4	6.88
	4695.44	6.53	-1.920	···	···	10.0	7.13	···	···	3.0	7.01	6.3	7.14	···	···	···	···

Table 9—Continued

	λ	χ		Kepler-20		Kepler-21		Kepler-22		Kepler-37		Kepler-68		Kepler-100		Kepler-130	
Ion	(Å)	(eV)	log gf	EW	log N	EW	log N	EW	log N	EW	log N	EW	log N	EW	log N	EW	log N
	6757.17	7.87	-0.310	...	...	...	...	...	...	4.0	6.82	19.0	7.29	27.8	7.43	11.7	6.98
K I	7698.98	0.00	-0.170	173.2	5.37	146.7	5.45	163.3	5.10	164.2	4.95	165.1	5.41	155.3	5.52	132.4	5.11
Ca I	5867.56	2.93	-1.570	34.3	6.37	15.3	6.28	20.3	6.12	22.8	6.05	26.9	6.42	24.1	6.36	12.4	6.05
	6161.30	2.52	-1.266	79.5	6.42	46.3	6.25	59.7	6.11	67.0	6.08	67.1	6.40	62.4	6.37	47.6	6.14
	6166.44	2.52	-1.142	84.4	6.37	53.1	6.23	64.7	6.06	70.3	6.01	75.3	6.40	69.4	6.36	56.6	6.15
	6169.04	2.52	-0.797	110.8	6.39	75.3	6.22	84.6	6.00	96.3	6.02	96.6	6.37	94.2	6.45	77.9	6.13
	6169.56	2.53	-0.478	130.1	6.30	93.7	6.18	107.0	5.97	116.6	5.95	116.5	6.33	111.3	6.42	96.6	6.10
	6572.78	0.00	-4.240	54.2	6.34	13.9	6.19	33.6	6.09	45.4	6.05	34.9	6.39	28.7	6.26	18.3	6.10
	7326.15	2.93	-0.208	125.4	6.26	92.4	6.18	106.1	5.99	112.6	5.94	118.2	6.35	112.6	6.44	...	...
Sc II	6245.64	1.51	-1.030	34.5	3.12	42.4	2.97	25.4	2.85	24.7	2.79	45.9	3.30	43.6	3.05	31.1	2.90
	6320.85	1.50	-1.819	9.0	3.13	9.8	2.95	5.9	2.89	04.5	2.72	11.6	3.27	...	...	...	...
	6604.60	1.36	-1.309	37.2	3.28	39.5	3.04	27.9	3.02	25.9	2.93	46.0	3.41	44.4	3.17	30.4	3.01
Ti I	5022.87	0.83	-0.434	91.0	4.96	52.5	4.76	73.1	4.60	79.0	4.49	80.2	4.99	71.6	4.87	56.8	4.63
	5024.84	0.82	-0.602	86.4	5.03	48.6	4.86	68.8	4.68	73.6	4.55	74.5	5.05	68.8	4.97	53.7	4.74
	5039.96	0.02	-1.130	93.7	4.87	56.3	4.76	75.3	4.51	82.3	4.39	80.5	4.89	76.2	4.84	60.9	4.61
	5210.39	0.05	-0.884	108.0	4.91	66.5	4.69	92.2	4.59	106.6	4.60	94.8	4.92	84.0	4.76	75.9	4.62
	5739.47	2.25	-0.600	16.2	4.95	3.3	4.73	7.4	4.66	10.2	4.63	09.4	4.98	6.9	4.82	3.4	4.57
	5866.45	1.07	-0.840	67.9	5.04	23.3	4.81	46.3	4.72	57.2	4.67	52.1	5.07	44.8	4.95	31.5	4.78
	6091.17	2.27	-0.423	26.1	5.04	...	...	13.1	4.76	17.0	4.71	17.9	5.13	12.2	4.92	9.6	4.87
	6258.10	1.44	-0.355	67.3	4.90	28.5	4.77	51.2	4.67	58.8	4.59	56.1	4.99	47.0	4.85	34.2	4.68
	6261.10	1.43	-0.479	69.0	5.04	26.9	4.85	47.4	4.72	57.1	4.67	55.1	5.09	48.9	4.99	30.6	4.72
	7138.91	1.44	-1.590	16.0	5.03			6.7	4.71	9.2	4.64	8.4	5.06	...	...	...	...
Ti II	4779.98	2.05	-1.260	63.0	4.95	78.1	4.75	55.9	4.68	52.6	4.60	73.5	5.03	...	...	...	...
	5154.07	1.57	-1.750	76.5	5.21	...	...	63.4	4.80	62.0	4.75	82.4	5.19	81.8	5.01	67.9	4.76
	5336.79	1.58	-1.590	70.4	4.92	88.2	4.76	61.4	4.60	58.3	4.53	82.2	5.02	80.1	4.81	70.1	4.64
	5381.02	1.57	-1.920	58.8	4.99	73.1	4.82	48.7	4.69	46.3	4.61	71.0	5.12	74.0	5.00	59.3	4.77
V I	5727.05	1.08	-0.012	63.9	4.17	16.4	3.82	36.3	3.73	47.1	3.70	42.4	4.10	34.1	3.94	18.6	3.67
	5737.06	1.06	-0.740	23.9	4.08	...	...	10.3	3.75	14.3	3.68	11.9	4.09	9.3	3.95	...	...
	6081.44	1.05	-0.579	26.6	3.95	5.9	3.85	13.5	3.69	17.3	3.58	16.4	4.06	12.1	3.88	...	...
	6090.21	1.08	-0.062	51.4	3.95	13.8	3.76	30.1	3.64	39.1	3.58	35.8	4.01	29.8	3.88	18.5	3.69
	6111.65	1.04	-0.715	24.3	4.02	...	...	11.0	3.71	15.3	3.65	12.4	4.04	...	...	...	...
	6224.53	0.29	-2.010	14.9	4.24	...	...	7.6	4.05	09.5	3.89	08.0	4.38	...	...	...	...
	6243.10	0.30	-0.980	57.6	4.14	...	...	29.6	3.73	43.0	3.72	31.4	4.07	...	...	13.4	3.68

Table 9—Continued

	λ	χ		Kepler-20		Kepler-21		Kepler-22		Kepler-37		Kepler-68		Kepler-100		Kepler-130	
Ion	(Å)	(eV)	log gf	EW	log N	EW	log N	EW	log N	EW	log N	EW	log N	EW	log N	EW	log N
	6251.83	0.29	-1.340	32.1	4.01	4.5	3.77	15.6	3.72	22.5	3.65	17.2	4.08	···	···	7.6	3.76
	6285.15	0.28	-1.510	24.2	3.99	···	···	10.9	3.70	22.0	3.80	11.1	4.02	9.5	3.92	···	···
Cr I	5702.31	3.45	-0.667	36.0	5.91	···	···	19.7	5.59	22.4	5.53	27.7	5.95	···	···	···	···
	5783.06	3.32	-0.500	42.0	5.73	17.3	5.57	25.5	5.44	27.9	5.36	34.2	5.79	27.9	5.66	16.3	5.40
	5783.85	3.32	-0.295	58.0	5.81	24.6	5.56	35.7	5.44	39.8	5.38	47.9	5.83	41.3	5.73	24.5	5.42
	5787.92	3.32	-0.083	57.3	5.58	29.8	5.45	38.6	5.28	42.5	5.21	49.7	5.64	···	···	···	···
	6330.09	0.94	-2.920	43.8	5.70	10.4	5.53	23.9	5.40	32.7	5.36	29.5	5.79	26.5	5.71	11.5	5.36
	6978.40	3.46	0.142	73.7	5.71	39.6	5.49	49.5	5.32	55.4	5.29	64.7	5.73	56.9	5.65	40.2	5.37
	6979.80	3.46	-0.410	48.4	5.84	19.3	5.62	27.7	5.49	29.5	5.39	41.0	5.90	34.8	5.80	17.4	5.43
	7400.25	2.90	-0.111	94.7	5.71	52.6	5.41	67.4	5.28	76.2	5.26	79.8	5.65	77.4	5.68	55.8	5.32
Mn I	5399.50	3.85	-0.287	55.8	5.73[b]	18.5	5.32	25.4	5.17	28.0	5.10	41.4	5.65	38.5	5.60	19.5	5.22
	5432.55	0.00	-3.795	83.5	5.84[b]	···	···	44.0	5.14	61.6	5.18[b]	50.7	5.57	45.1	5.46	22.0	5.11
Fe I	4779.44	3.42	-2.020	49.6	7.30	24.8	7.18	35.6	7.04	37.4	6.94	43.7	7.38	···	···	27.6	7.09
	4788.76	3.24	-1.760	73.8	7.35	51.1	7.24	58.4	7.01	63.6	6.97	69.4	7.40	68.3	7.43	50.7	7.09
	5054.64	3.64	-1.920	49.3	7.39	22.5	7.21	32.7	7.08	35.4	7.01	42.0	7.44	38.6	7.36	24.3	7.11
	5322.04	2.28	-2.800	70.9	7.31	40.1	7.19	54.3	6.98	60.3	6.92	64.3	7.38	···	···	45.3	7.09
	5379.57	3.69	-1.510	68.8	7.38	46.0	7.28	52.7	7.06	57.2	7.02	66.8	7.48	62.6	7.44	45.8	7.15
	5522.45	4.21	-1.550	50.8	7.58	29.8	7.49	36.7	7.32	36.8	7.22	45.3	7.63	40.8	7.55	27.3	7.31
	5543.94	4.22	-1.140	69.4	7.51	48.0	7.41	52.5	7.19	56.9	7.15	66.2	7.58	···	···	48.5	7.30
	5546.50	4.37	-1.310	58.8	7.63	38.4	7.55	41.7	7.32	45.1	7.28	56.3	7.72	52.7	7.68	36.3	7.40
	5546.99	4.22	-1.910	38.5	7.71	15.5	7.49	20.1	7.33	21.5	7.25	30.8	7.73	···	···	···	···
	5560.21	4.43	-1.190	60.0	7.59	36.9	7.46	43.4	7.29	45.6	7.23	56.7	7.66	···	···	···	···
	5577.03	5.03	-1.550	16.0	7.60	···	···	8.9	7.34	7.4	7.17	13.3	7.65	···	···	6.5	7.33
	5579.34	4.23	-2.400	14.5	7.62	···	···	7.2	7.31	9.3	7.32	11.1	7.67	···	···	···	···
	5587.57	4.14	-1.850	46.9	7.73	25.5	7.63	30.5	7.43	31.2	7.33	40.6	7.78	···	···	21.8	7.41
	5646.68	4.26	-2.500	12.3	7.66	···	···	5.9	7.35	7.3	7.34	09.9	7.74	7.7	7.60	···	···
	5651.47	4.47	-2.000	25.5	7.77	11.0	7.63	13.5	7.45	13.9	7.36	21.2	7.83	17.8	7.72	9.6	7.45
	5652.32	4.26	-1.950	34.3	7.70	15.2	7.56	19.9	7.40	21.0	7.32	29.3	7.77	25.1	7.66	13.8	7.38
	5661.35	4.28	-1.740	28.7	7.39	12.8	7.28	17.1	7.12	18.8	7.07	26.2	7.51	20.6	7.36	11.5	7.10
	5667.52	4.18	-1.580	62.0	7.77	33.2	7.55	41.4	7.40	43.7	7.33	56.0	7.80	···	···	33.2	7.43
	5677.68	4.10	-2.700	10.6	7.62	···	···	5.0	7.32	4.3	7.13	08.1	7.69	6.7	7.58	···	···
	5679.02	4.65	-0.920	67.7	7.65	43.5	7.49	50.1	7.33	51.0	7.25	64.2	7.71	61.6	7.71	45.2	7.41
	5680.24	4.19	-2.580	15.3	7.78	5.0	7.59	6.8	7.43	07.5	7.36	13.3	7.90	11.9	7.82	5.8	7.53

Table 9—Continued

	λ	χ		Kepler-20		Kepler-21		Kepler-22		Kepler-37		Kepler-68		Kepler-100		Kepler-130	
Ion	(Å)	(eV)	log gf	EW	log N	EW	log N	EW	log N	EW	log N	EW	log N	EW	log N	EW	log N
	5731.76	4.26	-1.300	67.0	7.66	41.8	7.50	50.0	7.34	52.3	7.28	62.4	7.70	···	···	43.5	7.41
	5732.27	4.99	-1.560	20.5	7.70	9.2	7.57	9.8	7.35	10.0	7.28	19.4	7.81	···	···	7.4	7.36
	5741.85	4.26	-1.850	39.9	7.71	19.3	7.58	24.5	7.41	27.2	7.36	35.7	7.79	32.4	7.72	18.6	7.43
	5752.03	4.55	-1.180	61.9	7.71	41.0	7.62	47.1	7.44	47.6	7.36	59.1	7.79	···	···	40.1	7.49
	5775.08	4.22	-1.300	68.9	7.65	43.3	7.49	50.7	7.31	53.1	7.25	63.8	7.69	59.3	7.65	42.8	7.36
	5778.45	2.59	-3.480	32.4	7.50	9.3	7.33	19.5	7.25	21.2	7.12	24.9	7.61	20.8	7.48	11.5	7.24
	5809.22	3.88	-1.840	60.9	7.72	31.5	7.50	40.0	7.34	45.0	7.31	56.0	7.78	47.5	7.64	30.8	7.36
	5934.65	3.93	-1.170	85.4	7.52	58.2	7.33	···	···	73.6	7.15	80.4	7.56	73.4	7.49	59.5	7.23
	6079.00	4.65	-1.120	54.1	7.61	33.7	7.51	37.4	7.31	36.9	7.20	50.0	7.66	···	···	32.5	7.38
	6085.26	2.76	-3.100	59.6	7.81	21.1	7.50	39.0	7.45	47.2	7.43	46.4	7.79	···	···	25.3	7.42
	6098.24	4.56	-1.880	22.4	7.64	···	···	11.4	7.32	10.9	7.20	19.8	7.73	15.2	7.58	8.5	7.34
	6151.62	2.18	-3.300	61.4	7.43	28.2	7.32	44.5	7.15	50.0	7.07	52.4	7.51	49.7	7.46	34.4	7.25
	6159.37	4.61	-1.970	16.7	7.62	6.3	7.45	9.1	7.35	09.4	7.26	13.9	7.68	11.1	7.55	6.2	7.32
	6165.36	4.14	-1.470	52.5	7.43	29.9	7.32	37.0	7.15	39.8	7.09	49.7	7.53	43.4	7.42	30.0	7.20
	6173.34	2.22	-2.880	80.5	7.42	47.6	7.27	61.9	7.06	67.7	6.99	71.8	7.45	65.3	7.35	52.1	7.17
	6187.99	3.94	-1.720	59.0	7.60	29.5	7.38	39.9	7.26	43.3	7.20	52.2	7.63	47.3	7.55	30.7	7.27
	6220.78	3.88	-2.460	···	···	11.6	7.57	14.6	7.35	15.3	7.25	22.4	7.74	···	···	···	···
	6226.73	3.88	-2.220	36.9	7.62	16.0	7.49	21.9	7.32	25.2	7.28	33.1	7.73	28.9	7.63	19.0	7.44
	6229.23	2.85	-2.810	46.9	7.36	24.3	7.36	30.4	7.07	37.1	7.05	45.3	7.55	37.6	7.40	24.6	7.20
	6240.65	2.22	-3.230	60.4	7.38	27.5	7.27	43.7	7.10	47.9	6.99	52.7	7.48	49.1	7.41	29.6	7.12
	6293.92	4.84	-1.720	···	···	9.3	7.58	9.6	7.34	11.0	7.32	16.6	7.73	···	···	···	···
	6297.79	2.22	-2.740	85.2	7.36	56.2	7.26	···	···	75.0	6.97	78.4	7.42	···	···	···	···
	6322.69	2.59	-2.430	86.0	7.44	56.0	7.29	···	···	73.5	7.02	80.2	7.50	···	···	59.8	7.19
	6380.74	4.19	-1.380	59.0	7.50	37.1	7.40	43.2	7.21	44.6	7.13	57.0	7.60	52.0	7.53	36.5	7.27
	6392.54	2.28	-4.030	27.9	7.59	6.6	7.40	14.4	7.29	18.7	7.24	18.8	7.66	16.4	7.56	8.2	7.30
	6597.56	4.79	-1.070	51.7	7.63	31.0	7.51	34.9	7.33	37.7	7.29	48.9	7.70	···	···	27.4	7.33
	6608.02	2.28	-4.030	27.5	7.57	7.8	7.46	14.3	7.27	18.1	7.21	21.3	7.71	17.5	7.58	8.4	7.30
	6609.11	2.56	-2.690	76.9	7.47	43.6	7.31	58.3	7.13	64.3	7.07	71.0	7.55	68.2	7.52	47.8	7.21
	6627.54	4.55	-1.680	34.8	7.69	16.0	7.53	20.3	7.38	23.0	7.35	31.3	7.77	26.1	7.65	16.7	7.44
	6653.85	4.15	-2.520	14.4	7.61	5.8	7.53	8.5	7.39	08.9	7.30	09.8	7.61	9.8	7.59	···	···
	6703.57	2.76	-3.160	48.2	7.61	···	···	31.6	7.33	34.6	7.23	42.0	7.73	35.4	7.59	21.8	7.37
	6710.32	1.49	-4.880	25.6	7.54	···	···	13.4	7.28	17.2	7.19	16.4	7.65	14.1	7.54	···	···
	6713.74	4.80	-1.600	26.2	7.67	···	···	15.6	7.40	15.4	7.31	25.5	7.79	21.0	7.67	11.7	7.41

Table 9—Continued

	λ	χ		Kepler-20		Kepler-21		Kepler-22		Kepler-37		Kepler-68		Kepler-100		Kepler-130	
Ion	(Å)	(eV)	log gf	EW	log N	EW	log N	EW	log N	EW	log N	EW	log N	EW	log N	EW	log N
	6716.22	4.58	-1.920	19.2	7.59	···	···	12.2	7.39	11.9	7.28	18.2	7.72	15.7	7.63	9.2	7.41
	6725.35	4.10	-2.300	25.8	7.66	···	···	12.8	7.31	14.5	7.26	21.4	7.73	16.8	7.58	8.3	7.29
	6726.67	4.61	-1.130	57.0	7.60	···	···	38.1	7.26	40.8	7.22	53.1	7.65	46.6	7.56	31.9	7.31
	6733.15	4.64	-1.580	34.5	7.67	···	···	19.8	7.35	20.1	7.26	29.9	7.72	26.1	7.63	···	···
	6739.52	1.56	-4.790	21.0	7.41	···	···	9.5	7.09	13.1	7.03	11.9	7.46	···	···	4.7	7.09
	6745.09	4.58	-2.160	···	···	···	···	4.7	7.18	6.0	7.19	09.8	7.65	···	···	···	···
	6745.96	4.08	-2.770	···	···	···	···	4.9	7.31	5.5	7.25	08.1	7.70	···	···	···	···
	6750.15	2.42	-2.620	86.7	7.43	···	···	···	···	75.8	7.04	79.1	7.46	···	···	···	···
	6752.72	4.64	-1.300	43.4	7.56	···	···	28.1	7.27	29.0	7.19	40.2	7.63	···	···	22.8	7.31
	7114.55	2.69	-4.010	14.2	7.58	3.7	7.46	6.0	7.23	10.0	7.30	08.7	7.62	8.0	7.55	···	···
	7284.84	4.14	-1.750	50.0	7.61	24.7	7.44	33.3	7.31	34.5	7.22	47.3	7.71	46.1	7.69	···	···
Fe II	4620.52	2.83	-3.315	47.8	7.47	66.8	7.29	37.7	7.12	35.3	7.10	60.2	7.55	64.3	7.45	47.8	7.16
	5197.58	3.23	-2.348	73.8	7.46	···	···	65.3	7.09	60.9	7.06	89.9	7.51	89.2	7.37	79.9	7.13
	5234.62	3.22	-2.279	75.8	7.43	101.6	7.19	67.8	7.05	61.1	6.99	91.4	7.46	93.7	7.39	78.9	7.02
	5264.81	3.23	-3.133	39.9	7.48	62.0	7.35	30.3	7.15	28.6	7.15	54.4	7.59	···	···	40.8	7.18
	5414.07	3.22	-3.645	22.5	7.53	38.4	7.44	17.2	7.29	13.6	7.19	36.6	7.73	37.2	7.54	23.5	7.31
	5425.26	3.20	-3.390	36.3	7.61	56.4	7.47	27.9	7.31	24.0	7.25	52.5	7.77	52.7	7.58	36.9	7.33
	6084.11	3.20	-3.881	18.5	7.62	30.1	7.46	11.5	7.28	08.8	7.17	17.5	7.46	28.4	7.54	18.5	7.37
	6113.32	3.22	-4.230	···	···	18.9	7.56	6.7	7.38	5.8	7.34	15.2	7.75	19.6	7.67	8.1	7.32
	6149.26	3.89	-2.841	30.2	7.58	51.7	7.44	24.2	7.32	20.0	7.26	46.0	7.72	46.3	7.53	32.4	7.31
	6239.95	3.89	-3.573	12.5	7.74	22.3	7.60	6.1	7.31	···	···	20.2	7.86	···	···	···	···
	6247.56	3.89	-2.435	45.3	7.55	75.4	7.43	37.8	7.24	31.5	7.17	61.5	7.62	65.9	7.52	51.5	7.27
	7222.39	3.89	-3.402	17.1	7.73	28.9	7.54	11.6	7.44	11.5	7.49	26.6	7.83	27.5	7.65	···	···
	7449.34	3.89	-3.488	14.6	7.72	30.0	7.64	12.3	7.54	08.9	7.43	24.7	7.86	···	···	13.0	7.38
	7711.72	3.90	-2.683	40.0	7.63	72.2	7.54	32.6	7.33	29.5	7.34	57.0	7.72	59.3	7.57	···	···
Co I	5301.04	1.71	-2.000	32.4	5.05	···	···	18.1	4.76	20.2	4.63	23.7	5.15	21.6	5.06	11.0	4.80
	5647.23	2.28	-1.560	24.3	4.99	4.6	4.66	11.5	4.64	14.7	4.60	16.6	5.05	13.5	4.90	6.9	4.66
	6595.86	3.71	-0.647	9.0	4.97	···	···	···	···	3.9	4.50	06.9	5.03	5.4	4.88	···	···
	6632.43	2.28	-2.000	···	···	···	···	8.8	4.90	8.5	4.72	11.4	5.24	···	···	···	···
	6678.80	1.96	-2.680	10.0	5.24	···	···	···	···	4.0	4.70	05.2	5.23	···	···	···	···
	6814.94	1.96	-1.900	32.0	5.10	7.7	4.88	16.4	4.77	20.5	4.71	20.5	5.12	19.9	5.06	9.5	4.77
Ni I	5748.35	1.68	-3.260	39.1	6.26	13.5	6.11	22.3	5.92	26.0	5.85	32.8	6.38	27.6	6.22	15.6	5.99
	5754.65	1.94	-2.330	88.8	6.59	···	···	68.1	6.12	73.7	6.08	83.1	6.59	···	···	···	···

Table 9—Continued

	λ	χ		Kepler-20		Kepler-21		Kepler-22		Kepler-37		Kepler-68		Kepler-100		Kepler-130	
Ion	(Å)	(eV)	log gf	EW	log N	EW	log N	EW	log N	EW	log N	EW	log N	EW	log N	EW	log N
	5760.83	4.11	-0.800	42.3	6.31	22.8	6.14	25.1	5.95	25.2	5.88	38.9	6.36	34.8	6.26	21.9	6.01
	5805.21	4.17	-0.640	48.4	6.33	27.4	6.14	31.3	5.99	31.4	5.91	48.0	6.42	47.4	6.40	26.0	6.01
	5846.99	1.68	-3.210	33.7	6.09	9.9	5.91	18.3	5.76	21.7	5.69	27.0	6.20	···	···	···	···
	6108.11	1.68	-2.450	76.9	6.17	40.6	5.90	57.7	5.77	61.9	5.69	68.8	6.17	···	···	···	···
	6111.07	4.09	-0.870	42.0	6.35	21.6	6.15	26.2	6.02	24.5	5.90	38.3	6.39	35.4	6.31	19.5	5.99
	6128.96	1.68	-3.330	35.2	6.22	12.5	6.12	20.0	5.91	23.1	5.83	28.1	6.33	22.7	6.16	16.0	6.05
	6130.13	4.27	-0.960	26.8	6.30	13.5	6.16	15.2	5.98	14.0	5.87	25.1	6.37	23.7	6.31	15.1	6.11
	6133.96	4.09	-1.830	8.5	6.37	···	···	3.5	5.98	4.5	6.01	08.2	6.50	···	···	···	···
	6175.36	4.09	-0.559	53.4	6.25	37.1	6.17	39.0	5.96	38.5	5.88	52.6	6.32	53.1	6.34	35.5	6.03
	6176.81	4.09	-0.260	70.1	6.25	47.3	6.04	52.2	5.89	52.4	5.82	69.8	6.31	66.5	6.29	46.7	5.93
	6177.24	1.83	-3.500	23.0	6.27	···	···	11.4	5.94	12.4	5.82	16.0	6.33	15.9	6.28	6.7	5.95
	6186.71	4.11	-0.960	39.4	6.40	18.2	6.16	21.5	6.01	22.2	5.95	35.2	6.43	31.1	6.33	18.0	6.05
	6204.60	4.09	-1.100	28.5	6.30	12.4	6.09	14.7	5.93	15.6	5.88	23.9	6.31	24.8	6.30	11.3	5.93
	6223.98	4.11	-0.910	33.8	6.24	16.8	6.07	21.2	5.95	20.0	5.84	32.1	6.32	28.9	6.23	18.2	6.00
	6230.09	4.11	-1.260	27.4	6.45	11.5	6.23	14.6	6.10	17.0	6.10	24.5	6.50	25.1	6.49	12.2	6.15
	6327.59	1.68	-3.150	51.0	6.34	17.6	6.10	32.7	6.01	36.5	5.92	43.1	6.42	37.9	6.28	25.0	6.10
	6370.34	3.54	-1.940	17.8	6.31	7.8	6.21	9.0	5.98	09.0	5.88	14.5	6.36	14.1	6.31	6.5	5.99
	6378.25	4.15	-0.830	38.2	6.29	20.2	6.13	23.0	5.96	22.4	5.87	37.5	6.38	32.8	6.27	21.9	6.06
	6598.59	4.24	-0.980	29.2	6.33	14.4	6.17	17.2	6.02	16.4	5.92	29.8	6.45	27.6	6.38	18.0	6.17
	6635.12	4.42	-0.820	28.8	6.33	16.1	6.22	16.5	6.02	14.8	5.89	27.6	6.41	29.6	6.43	13.9	6.05
	6643.63	1.68	-2.300	106.4	6.49	67.7	6.13	86.0	6.06	90.6	5.99	98.5	6.47	96.5	6.48	72.6	6.05
	6767.77	1.83	-2.170	87.1	6.17	···	···	71.9	5.83	···	···	···	···	79.3	6.16	62.5	5.90
	6842.03	3.66	-1.480	32.5	6.31	14.9	6.15	20.4	6.03	19.4	5.91	28.4	6.36	30.5	6.37	15.2	6.03
Zn I	4722.15	4.03	-0.338	69.4	4.56	65.6	4.24	56.5	4.15	56.0	4.15	77.5	4.60	79.3	4.62	61.7	4.20

[a]Not corrected for Ni blend

[b]Not corrected for hfs

Table 10. Solar Lines Measured, Equivalent Widths, and Abundances

	λ	χ		Kepler-20, Kepler-21, Kepler-22		Kepler-37, Kepler-68		Kepler-100, Kepler-130	
Ion	(Å)	(eV)	log gf	$EW_\odot$	$\log N_\odot$	$EW_\odot$	$\log N_\odot$	$EW_\odot$	$\log N_\odot$
C I	5052.17	7.68	-1.304	31.7	8.41	32.3	8.43	33.2	8.46
	5380.34	7.68	-1.615	19.5	8.44	20.2	8.46	19.4	8.45
	6587.61	8.54	-1.021	14.1	8.42	16.4	8.51	13.1	8.39
	7111.47	8.64	-1.074	9.4	8.36	13.3	8.54	10.5	8.42
	7113.18	8.65	-0.762	23.3	8.56	24.7	8.60	21.9	8.54
O I	6300.30[a]	0.00	-9.720	5.6	8.68	...	...		
	7771.94	9.15	0.369	71.2	8.86	68.5	8.81	65.6	8.80
	7774.17	9.15	0.223	64.8	8.90	61.7	8.85	58.7	8.83
	7775.39	9.15	0.001	45.0	8.78	42.5	8.73	39.6	8.68
Na I	5682.63	2.10	-0.700	99.5	6.29	103.0	6.33	106.2	6.42
	6154.23	2.10	-1.560	37.5	6.29	36.9	6.28	32.0	6.20
	6160.75	2.10	-1.260	57.5	6.30	55.6	6.27	53.2	6.25
Mg I	4730.03	4.35	-2.523	69.0	7.84	72.4	7.89	55.9	7.68
	5711.09	4.35	-1.833	104.4	7.60	104.4	7.60	101.4	7.61
	6965.41	5.75	-1.510	22.9	7.27	22.1	7.25	...	...
Al I	6696.02	3.14	-1.347	37.7	6.26	37.7	6.26	36.7	6.25
	6698.67	3.14	-1.647	20.9	6.22	20.2	6.20	20.3	6.21
Si I	5690.43	4.93	-1.769	51.4	7.50	51.1	7.49	49.2	7.48
	5701.10	4.93	-1.581	38.3	7.10	37.6	7.08	...	...
	5708.40	4.95	-1.034	75.4	7.13	76.3	7.14	...	...
	5772.15	5.08	-1.358	52.5	7.24	52.5	7.24	...	...
	6125.02	5.61	-1.464	32.5	7.48	32.2	7.48	29.0	7.42
	6142.48	5.62	-1.295	35.3	7.36	34.2	7.34	31.0	7.30
	6145.02	5.62	-1.310	39.5	7.45	38.5	7.43	36.3	7.41
	6243.81	5.62	-1.242	48.4	7.52	47.6	7.51	48.5	7.54
	6244.47	5.62	-1.093	46.8	7.35	46.2	7.34	46.7	7.36
	6414.98	5.87	-1.035	46.7	7.48	48.5	7.51	38.3	7.37
	6741.63	5.98	-1.428	14.7	7.33	14.3	7.32	14.8	7.34
	6848.58	5.86	-1.524	17.9	7.42	17.4	7.41	15.3	7.35
	7003.57	5.96	-0.937	58.4	7.62	58.7	7.62	...	...
	7405.77	5.61	-0.313	90.6	7.11	89.3	7.10	...	...
S I	4694.11	6.53	-1.770	15.6	7.50	11.9	7.35	9.6	7.24
	4695.44	6.53	-1.920	7.5	7.26	5.0	7.07	...	...

Table 10—Continued

	λ	χ		Kepler-20, Kepler-21, Kepler-22		Kepler-37, Kepler-68		Kepler-100, Kepler-130	
Ion	(Å)	(eV)	log gf	$EW_\odot$	$\log N_\odot$	$EW_\odot$	$\log N_\odot$	$EW_\odot$	$\log N_\odot$
	6757.17	7.87	-0.310	16.0	7.26	14.3	7.19	16.5	7.29
K I	7698.98	0.00	-0.170	168.3	5.38	157.3	5.28	152.7	5.31
Ca I	5867.56	2.93	-1.570	24.2	6.30	24.2	6.30	21.5	6.24
	6161.30	2.52	-1.266	64.9	6.33	63.5	6.30	61.6	6.29
	6166.44	2.52	-1.142	69.8	6.28	68.7	6.26	69.3	6.29
	6169.04	2.52	-0.797	93.4	6.29	92.2	6.28	93.1	6.33
	6169.56	2.53	-0.478	112.3	6.24	111.7	6.23	111.2	6.29
	6572.78	0.00	-4.240	34.4	6.28	32.4	6.24	30.9	6.21
	7326.15	2.93	-0.208	108.8	6.20	110.2	6.21	110.7	6.28
Sc II	6245.64	1.51	-1.030	35.8	3.09	35.1	3.07	34.6	3.07
	6320.85	1.50	-1.819	8.5	3.07	8.0	3.04	...	...
	6604.60	1.36	-1.309	36.3	3.21	36.7	3.22	34.0	3.17
Ti I	5022.87	0.83	-0.434	74.3	4.83	76.4	4.88	73.1	4.82
	5024.84	0.82	-0.602	68.9	4.89	70.4	4.92	62.9	4.78
	5039.96	0.02	-1.130	74.7	4.72	75.6	4.74	68.3	4.61
	5210.39	0.05	-0.884	89.9	4.79	88.3	4.76	86.4	4.74
	5739.47	2.25	-0.600	8.1	4.82	8.4	4.84	7.2	4.77
	5866.45	1.07	-0.840	47.5	4.91	48.2	4.92	41.5	4.81
	6091.17	2.27	-0.423	14.5	4.93	14.7	4.94	13.9	4.91
	6258.10	1.44	-0.355	51.5	4.84	50.8	4.83	50.0	4.82
	6261.10	1.43	-0.479	48.9	4.91	48.3	4.90	47.5	4.89
	7138.91	1.44	-1.590	7.0	4.88	6.7	4.86	...	...
Ti II	4779.98	2.05	-1.260	64.0	4.86	64.7	4.87	38.3	4.35
	5154.07	1.57	-1.750	75.5	5.08	74.5	5.06	70.3	4.98
	5336.79	1.58	-1.590	72.1	4.85	71.8	4.84	67.9	4.77
	5381.02	1.57	-1.920	59.9	4.92	59.6	4.92	59.7	4.92
V I	5727.05	1.08	-0.012	39.7	3.96	39.4	3.96	37.4	3.92
	5737.06	1.06	-0.740	10.4	3.91	10.5	3.92	9.4	3.86
	6081.44	1.05	-0.579	14.0	3.87	14.2	3.87	11.7	3.78
	6090.21	1.08	-0.062	33.2	3.87	33.0	3.86	32.4	3.85
	6111.65	1.04	-0.715	11.9	3.91	11.3	3.89	...	...
	6224.53	0.29	-2.010	7.9	4.25	7.7	4.23	4.8	4.01
	6243.10	0.30	-0.980	31.2	3.95	29.0	3.90	28.1	3.89

Table 10—Continued

	λ	χ		Kepler-20, Kepler-21, Kepler-22		Kepler-37, Kepler-68		Kepler-100, Kepler-130	
Ion	(Å)	(eV)	log gf	$EW_\odot$	$\log N_\odot$	$EW_\odot$	$\log N_\odot$	$EW_\odot$	$\log N_\odot$
	6251.83	0.29	-1.340	15.7	3.91	15.4	3.90	15.1	3.89
	6285.15	0.28	-1.510	11.3	3.90	10.8	3.88	9.2	3.80
Cr I	5702.31	3.45	-0.667	27.6	5.88	24.8	5.82	...	...
	5783.06	3.32	-0.500	30.9	5.66	30.6	5.66	28.8	5.63
	5783.85	3.32	-0.295	43.6	5.70	43.2	5.69	41.0	5.66
	5787.92	3.32	-0.083	45.7	5.52	45.1	5.51	...	...
	6330.09	0.94	-2.920	26.9	5.64	27.2	5.64	27.1	5.64
	6978.40	3.46	0.142	59.6	5.61	59.7	5.61	52.9	5.51
	6979.80	3.46	-0.410	36.4	5.76	36.0	5.76	32.2	5.69
	7400.25	2.90	-0.111	75.5	5.56	74.9	5.55	73.7	5.55
Mn I	5399.50	3.85	-0.287	40.2	5.57	38.1	5.53	36.7	5.51
	5432.55	0.00	-3.795	52.3	5.49	51.3	5.48	48.3	5.43
Fe I	4779.44	3.42	-2.020	40.3	7.25	40.9	7.26	39.8	7.25
	4788.76	3.24	-1.760	65.5	7.30	66.3	7.31	67.2	7.35
	5054.64	3.64	-1.920	39.1	7.32	39.7	7.33	36.2	7.27
	5322.04	2.28	-2.800	59.1	7.23	60.4	7.26	60.5	7.27
	5379.57	3.69	-1.510	60.5	7.33	61.0	7.34	59.1	7.33
	5522.45	4.21	-1.550	43.7	7.55	43.5	7.55	43.0	7.55
	5543.94	4.22	-1.140	62.1	7.47	62.3	7.48	62.1	7.50
	5546.50	4.37	-1.310	51.3	7.59	51.6	7.60	52.1	7.63
	5546.99	4.22	-1.910	28.4	7.62	28.3	7.62	30.2	7.66
	5560.21	4.43	-1.190	51.6	7.54	51.6	7.54	63.0	7.76
	5577.03	5.03	-1.550	10.8	7.50	10.8	7.50	10.8	7.50
	5579.34	4.23	-2.400	11.3	7.61	12.0	7.64	13.3	7.70
	5587.57	4.14	-1.850	37.8	7.67	37.9	7.67	33.3	7.59
	5646.68	4.26	-2.500	7.9	7.57	8.0	7.58	8.2	7.59
	5651.47	4.47	-2.000	18.3	7.69	18.2	7.69	16.7	7.64
	5652.32	4.26	-1.950	26.3	7.65	26.2	7.64	25.2	7.63
	5661.35	4.28	-1.740	22.5	7.36	21.7	7.34	22.1	7.36
	5667.52	4.18	-1.580	51.5	7.69	50.8	7.67	49.9	7.67
	5677.68	4.10	-2.700	6.6	7.53	7.0	7.56	6.3	7.51
	5679.02	4.65	-0.920	58.8	7.58	59.6	7.60	59.9	7.63
	5680.24	4.19	-2.580	10.2	7.70	10.5	7.72	10.3	7.71

Table 10—Continued

	λ	χ		Kepler-20, Kepler-21, Kepler-22		Kepler-37, Kepler-68		Kepler-100, Kepler-130	
Ion	(Å)	(eV)	log gf	$EW_\odot$	$\log N_\odot$	$EW_\odot$	$\log N_\odot$	$EW_\odot$	$\log N_\odot$
	5731.76	4.26	-1.300	58.1	7.60	58.3	7.60	56.5	7.59
	5732.27	4.99	-1.560	14.9	7.63	14.6	7.62	13.5	7.58
	5741.85	4.26	-1.850	32.0	7.67	30.9	7.64	32.6	7.68
	5752.03	4.55	-1.180	55.2	7.69	54.0	7.67	53.7	7.68
	5775.08	4.22	-1.300	58.8	7.57	59.1	7.57	58.1	7.58
	5778.45	2.59	-3.480	22.3	7.45	21.7	7.44	20.4	7.40
	5809.22	3.88	-1.840	48.2	7.60	48.3	7.60	47.4	7.59
	5934.65	3.93	-1.170	76.5	7.47	76.3	7.46	71.7	7.41
	6079.00	4.65	-1.120	45.7	7.55	46.7	7.57	43.3	7.52
	6085.26	2.76	-3.100	43.3	7.66	43.1	7.66	44.1	7.68
	6098.24	4.56	-1.880	15.9	7.56	16.3	7.57	13.8	7.49
	6151.62	2.18	-3.300	49.7	7.40	49.2	7.39	48.6	7.38
	6159.37	4.61	-1.970	12.6	7.58	12.7	7.58	11.4	7.53
	6165.36	4.14	-1.470	44.5	7.39	44.2	7.39	42.8	7.37
	6173.34	2.22	-2.880	67.5	7.33	67.6	7.33	67.4	7.34
	6187.99	3.94	-1.720	47.6	7.51	48.3	7.52	46.5	7.50
	6220.78	3.88	-2.460	20.2	7.62	20.4	7.62	18.7	7.58
	6226.73	3.88	-2.220	29.3	7.59	28.9	7.59	28.5	7.58
	6229.23	2.85	-2.810	37.5	7.34	40.7	7.40	39.4	7.38
	6240.65	2.22	-3.230	49.1	7.35	49.4	7.35	50.7	7.38
	6293.92	4.84	-1.720	13.6	7.58	14.1	7.60	11.2	7.49
	6297.79	2.22	-2.740	73.7	7.30	74.0	7.30	73.1	7.30
	6322.69	2.59	-2.430	76.0	7.39	75.8	7.39	74.2	7.37
	6380.74	4.19	-1.380	51.3	7.46	52.5	7.48	50.9	7.47
	6392.54	2.28	-4.030	17.6	7.53	18.3	7.55	16.4	7.50
	6597.56	4.79	-1.070	43.2	7.56	43.2	7.56	41.8	7.55
	6608.02	2.28	-4.030	17.3	7.51	17.7	7.52	17.2	7.51
	6609.11	2.56	-2.690	65.3	7.41	64.9	7.40	66.5	7.44
	6627.54	4.55	-1.680	28.0	7.65	27.7	7.64	25.8	7.60
	6653.85	4.15	-2.520	10.0	7.55	10.6	7.58	8.7	7.49
	6703.57	2.76	-3.160	36.9	7.56	37.7	7.58	35.3	7.54
	6710.32	1.49	-4.880	15.8	7.52	16.1	7.53	14.6	7.48
	6713.74	4.80	-1.600	21.1	7.64	21.3	7.64	19.6	7.60

Table 10—Continued

	λ	χ		Kepler-20, Kepler-21, Kepler-22		Kepler-37, Kepler-68		Kepler-100, Kepler-130	
Ion	(Å)	(eV)	log gf	$EW_\odot$	$\log N_\odot$	$EW_\odot$	$\log N_\odot$	$EW_\odot$	$\log N_\odot$
	6716.22	4.58	-1.920	15.2	7.57	15.2	7.57	15.1	7.57
	6725.35	4.10	-2.300	18.0	7.58	18.5	7.59	16.8	7.54
	6726.67	4.61	-1.130	46.8	7.51	47.0	7.51	46.3	7.51
	6733.15	4.64	-1.580	27.0	7.61	27.7	7.62	25.6	7.58
	6739.52	1.56	-4.790	11.6	7.34	11.7	7.35	11.1	7.32
	6745.09	4.58	-2.160	8.9	7.55	8.7	7.53	8.2	7.51
	6745.96	4.08	-2.770	8.3	7.64	7.4	7.59	6.8	7.55
	6750.15	2.42	-2.620	74.6	7.35	73.9	7.34	73.1	7.34
	6752.72	4.64	-1.300	36.4	7.52	36.6	7.52	35.1	7.50
	7114.55	2.69	-4.010	8.3	7.50	8.7	7.53	7.4	7.45
	7284.84	4.14	-1.750	41.6	7.56	41.8	7.57	38.4	7.51
Fe II	4620.52	2.83	-3.315	52.6	7.42	53.5	7.44	46.7	7.30
	5197.58	3.23	-2.348	79.4	7.37	79.9	7.38	76.2	7.32
	5234.62	3.22	-2.279	81.6	7.33	82.6	7.35	81.2	7.35
	5264.81	3.23	-3.133	45.3	7.43	45.6	7.44	39.5	7.31
	5414.07	3.22	-3.645	27.3	7.53	29.8	7.59	27.2	7.53
	5425.26	3.20	-3.390	40.1	7.54	42.3	7.59	38.6	7.51
	6084.11	3.20	-3.881	20.9	7.56	22.0	7.59	19.3	7.51
	6113.32	3.22	-4.230	11.7	7.60	12.5	7.64	12.1	7.62
	6149.26	3.89	-2.841	36.3	7.55	35.7	7.54	34.9	7.52
	6239.95	3.89	-3.573	13.5	7.64	12.3	7.59	7.2	7.32
	6247.56	3.89	-2.435	50.9	7.46	52.0	7.48	46.5	7.37
	7222.39	3.89	-3.402	19.5	7.65	19.8	7.66	17.5	7.59
	7449.34	3.89	-3.488	18.5	7.70	20.5	7.76	15.0	7.58
	7711.72	3.90	-2.683	47.2	7.57	45.8	7.55	43.6	7.50
Co I	5301.04	1.71	-2.000	20.9	4.98	20.3	4.97	16.8	4.86
	5647.23	2.28	-1.560	14.5	4.89	14.6	4.89	14.2	4.88
	6595.86	3.71	-0.647	6.5	4.93	5.5	4.86	6.1	4.90
	6632.43	2.28	-2.000	11.6	5.16	8.5	5.01	6.2	4.86
	6678.80	1.96	-2.680	5.1	5.12	4.4	5.06	...	...
	6814.94	1.96	-1.900	19.9	5.00	19.7	5.00	17.3	4.93
Ni I	5748.35	1.68	-3.260	29.5	6.22	29.8	6.23	27.3	6.18
	5754.65	1.94	-2.330	75.7	6.43	75.8	6.43	...	...

Table 10—Continued

	λ	χ		Kepler-20, Kepler-21, Kepler-22		Kepler-37, Kepler-68		Kepler-100, Kepler-130	
Ion	(Å)	(eV)	log gf	$EW_\odot$	$\log N_\odot$	$EW_\odot$	$\log N_\odot$	$EW_\odot$	$\log N_\odot$
	5760.83	4.11	-0.800	35.7	6.25	36.0	6.26	31.3	6.17
	5805.21	4.17	-0.640	43.0	6.29	43.5	6.30	39.0	6.23
	5846.99	1.68	-3.210	22.6	6.01	22.2	6.00	...	...
	6108.11	1.68	-2.450	65.6	6.06	65.8	6.07	...	...
	6111.07	4.09	-0.870	36.1	6.30	35.0	6.28	33.1	6.25
	6128.96	1.68	-3.330	25.5	6.18	24.9	6.16	24.0	6.14
	6130.13	4.27	-0.960	22.0	6.25	21.3	6.23	22.0	6.25
	6133.96	4.09	-1.830	6.1	6.30	5.3	6.24	...	...
	6175.36	4.09	-0.559	48.6	6.22	48.7	6.22	50.3	6.27
	6176.81	4.09	-0.260	63.7	6.18	64.6	6.20	64.7	6.23
	6177.24	1.83	-3.500	15.7	6.23	15.6	6.22	15.2	6.21
	6186.71	4.11	-0.960	31.7	6.32	30.7	6.29	29.1	6.27
	6204.60	4.09	-1.100	21.7	6.21	21.3	6.20	20.2	6.17
	6223.98	4.11	-0.910	28.8	6.20	29.4	6.22	25.4	6.13
	6230.09	4.11	-1.260	21.2	6.37	22.2	6.40	17.7	6.27
	6327.59	1.68	-3.150	39.6	6.28	38.8	6.26	36.6	6.22
	6370.34	3.54	-1.940	14.5	6.30	12.7	6.23	13.2	6.25
	6378.25	4.15	-0.830	31.8	6.23	31.4	6.22	28.8	6.17
	6598.59	4.24	-0.980	24.9	6.29	24.8	6.29	22.2	6.23
	6635.12	4.42	-0.820	26.1	6.33	24.7	6.30	22.8	6.26
	6643.63	1.68	-2.300	94.0	6.38	93.6	6.37	87.9	6.29
	6767.77	1.83	-2.170	79.0	6.12	...	...	76.8	6.10
	6842.03	3.66	-1.480	27.7	6.29	26.8	6.27	23.9	6.20
Zn I	4722.15	4.03	-0.338	69.8	4.47	72.5	4.53	67.0	4.44

[a]Not corrected for Ni blend

[b]Not corrected for hfs